Mouse and Human Antibodies that Bind HLA-E-Leader Peptide Complexes and Enhance NK Cell Cytotoxicity

Dapeng Li[1,5,8,9,*], Simon Brackenridge[2,8], Lucy C. Walters[2,8], Olivia Swanson[1], Karl Harlos[3], Daniel Rozbesky[3,4], Derek W. Cain[1,5], Kevin Wiehe[1,5], Richard M. Scearce[1], Maggie Barr[1], Zekun Mu[1], Robert Parks[1], Max Quastel[2], Robert J. Edwards[1,5], Yunfei Wang[1,5], Wes Rountree[1,5], Kevin O. Saunders[1,6,7], Guido Ferrari[7], Persephone Borrow[2], E. Yvonne Jones[3], S. Munir Alam[1,5], Mihai L. Azoitei[1,5,*], Geraldine M. Gillespie[2,*], Andrew J. McMichael[2,*], Barton F. Haynes[1,6,*]

[1]Duke Human Vaccine Institute, Duke University School of Medicine, Durham, NC 27710, USA

[2]Nuffield Department of Clinical Medicine, University of Oxford, Oxford, OX3 7FZ, UK

[3]Division of Structural Biology, Wellcome Centre for Human Genetics, University of Oxford, Oxford, OX3 7BN, UK

[4]Department of Cell Biology, Charles University, Prague, 12800, Czech Republic

[5]Department of Medicine, Duke University School of Medicine, Durham, NC 27710, USA

[6]Department of Immunology, Duke University School of Medicine, Durham, NC 27710, USA

[7]Department of Surgery, Duke University School of Medicine, Durham, NC 27710, USA

[8]Authors contributed equally

[9]Lead contact

*Address correspondence to dapeng.li@duke.edu, mihai.azoitei@duke.edu, geraldine.gillespie@ndm.ox.ac.uk, andrew.mcmichael@ndm.ox.ac.uk and barton.haynes@duke.edu

ABSTRACT (155 words)

HLA-E is a non-classical class Ib molecule that has limited polymorphism and binds HLA class Ia leader peptides (VL9). HLA-E-VL9 complexes interact with the natural killer (NK) cell receptors NKG2A-C/CD94 and regulate NK cell-mediated cytotoxicity. Here we isolated a murine IgM antibody 3H4, that specifically recognized HLA-E-VL9 bound complexes and enhanced killing of HLA-E-VL9-expressing cells by an NKG2A^{+} NK cell line. Structural analysis revealed how 3H4 prevents CD94/NKG2A docking on HLA-E-VL9 by binding with an overlapping footprint. Upon *in vitro* maturation, an affinity-optimized 3H4 IgG showed enhanced NK killing of HLA-E-VL9-expressing cells. Remarkably, HLA-E-VL9-specific IgM autoantibodies with similar specificity and functions to 3H4 were subsequently isolated from naïve B cells of cytomegalovirus (CMV)-negative, healthy male human donors. Thus, a repertoire of germline low affinity HLA-E-VL9-reactive antibodies are present in both naïve human and murine B cell repertoires. These antibodies can enhance NK cell cytotoxicity and therefore have potential for therapeutic modulation of NK cell function.

40 **INTRODUCTION**

41 Natural killer (NK) cells play critical roles in immune surveillance by discriminating normal
42 from altered cells, and function by killing non-self malignant or pathogen-infected cells and by
43 producing inflammatory cytokines (Chiossone et al., 2018; Raulet, 2006; Yokoyama and Kim,
44 2006). Specific recognition of abnormal cells by NK cells relies on a series of activating and
45 inhibitory receptors, including the killer immunoglobulin-like receptor (KIR) family in humans and
46 NKG2/CD94 heterodimeric receptors (Andre et al., 2018; Chiossone et al., 2018). NK cell
47 inhibitory receptors ligate human lymphocyte antigen (HLA) or major histocompatibility complex
48 (MHC) class I molecules expressed on healthy cells as self. Conversely, cells lacking MHC
49 class I are recognized by NK cells as "missing-self" and are sensitive to NK cell-mediated killing
50 (Ljunggren and Karre, 1985, 1990). In humans, KIRs recognize specific classical HLA class Ia
51 molecules (Colonna and Samaridis, 1995; Karlhofer et al., 1992; Pende et al., 2019), whereas
52 the inhibitory NKG2A/CD94 heterodimeric receptor interacts with the non-classical HLA class Ib
53 molecule HLA-E and is balanced by an activating receptor NKG2C/CD94 (Braud et al., 1997;
54 Braud et al., 1998; Brooks et al., 1997). While KIR expression is heterogeneous, NKG2A/CD94
55 is expressed on ~40% of human NK cells (Andre et al., 1999; Mahapatra et al., 2017; Pende et
56 al., 2019). Unlike classical HLA class I molecules, HLA-E has limited polymorphism with only
57 two expressed variants, HLA-E*01:01 and HLA-E*01:03, that differ only in residue 107, which is
58 outside the peptide-binding groove (Kraemer et al., 2014). The NKG2A/CD94/HLA-E pathway is
59 an important immune checkpoint and has recently become a focus for NK cell-based
60 immunotherapeutic strategies (Andre et al., 2018; Hu et al., 2019; Kim et al., 2019; Souza-
61 Fonseca-Guimaraes et al., 2019; van Hall et al., 2019). A subset of CD8+ T cells also express
62 NKG2A/CD94, and inhibition of the NKG2A/CD94 - HLA-E interaction has similar application in
63 CD8+ T cell-based immunotherapy (Andre et al., 2018; van Montfoort et al., 2018).

64 HLA-E engages with NKG2A/CD94 via a restricted subset of peptides VMAPRT(L/V)
65 (V/L/I/F)L (designated VL9) that derive from the leader sequence of HLA-A, -C, -G and a third of

66 HLA-B molecules (Braud et al., 1997; Braud et al., 1998; Lee et al., 1998a; Lee et al., 1998b).
67 HLA-E binds VL9 peptides stabilizing its surface expression (Braud et al., 1997; Braud et al.,
68 1998). This indicates that HLA-Ia expression is not perturbed by a pathogenic process and
69 initiates recognition by NKG2A/CD94 or NKG2C/CD94 on NK cells. The binding affinity of HLA-
70 E-VL9 peptide complexes for NKG2A/CD94 is greater than that for NKG2C/CD94, so that the
71 inhibitory signal dominates to suppress aberrant NK cell-mediated cytotoxicity and cytokine
72 production (Aldrich et al., 1994; Braud et al., 1998; Kaiser et al., 2008; Llano et al., 1998; Rolle
73 et al., 2018). As a secondary function, HLA-E and its murine and rhesus macaque homologs are
74 capable of binding to a range of other host- and pathogen-derived peptides, including heat-
75 shock protein 60 (Hsp60)-derived peptides (Michaelsson et al., 2002), Mycobacterium
76 tuberculosis (Mtb) peptides (Joosten et al., 2010; van Meijgaarden et al., 2015), and simian
77 immunodeficiency virus (SIV) Gag peptides (Hansen et al., 2016; Walters et al., 2018).
78 However, the VL9 peptide binds HLA-E with higher affinity and dominates the peptidome
79 (McMurtrey et al., 2017). Only HLA-E-VL9 can engage CD94/NKG2A to protect cells from NK
80 cell cytotoxicity (Kraemer et al., 2015; Michaelsson et al., 2002; Sensi et al., 2009). Hence,
81 leader sequence VL9 peptides are essential not only for stabilizing HLA-E surface expression
82 but also for mediating HLA-E/NKG2A/CD94 regulation of NK cell self-recognition.
83 Natural autoantibodies are a specific class of antibodies that recognize self molecules and
84 populate the B cell germline repertoire in healthy individuals. These antibodies mostly comprise
85 non-mutated IgM isotypes and can participate in diverse immune functions ranging from
86 immune defense and regulation to immune pathology. Autoantibodies that recognize both
87 classical HLA-Ia (Alberu et al., 2007; Morales-Buenrostro et al., 2008) and HLA-E heavy chains
88 (Ravindranath et al., 2010a; Ravindranath et al., 2010b) have been reported previously. In
89 certain instances these antibodies have been implicated as contributors to allograft damage in
90 non-alloimmunised individuals (Hickey et al., 2016; McKenna et al., 2000). However, very little is
91 unknown beyond this, especially in relation to their frequencies, specificities and functions.

92 Here, we focused on HLA-E, and initially isolated a murine IgM monoclonal antibody (mAb)
93 3H4 that bound specifically to HLA-E-VL9 on target cells and enhanced NK cytotoxicity
94 mediated by an NKG2A+ NK cell line. Crystallographic analysis showed that 3H4 and
95 CD94/NKG2A cannot simultaneously bind to HLA-E-VL9 and that the heavy chain CDR3
96 residues at the 3H4-HLA-E-VL9 binding interface were germline-encoded. While 3H4 mAb
97 enhanced NK cytotoxicity as an IgM, the IgG form of the antibody did not. However,
98 mutagenized 3H4 IgG variants with enhanced HLA-E-VL9 binding affinity blocked NKG2A
99 mediated inhibition of NK cells. We subsequently screened healthy humans blood donors and
100 identified HLA-E-VL9-reactive, near-germline IgMs autoantibodies from human naïve B cell
101 repertoires. Some of these antibodies also enhanced NK cell killing as IgG subtypes. Thus, we
102 identified a group of near germline HLA-E-VL9-targeting antibodies in mice and male CMV
103 seronegative humans that have the potential to regulate NK cell function.
104
105 **RESULTS**
106 **Isolation of murine HLA-E-VL9-specific mAb 3H4**
107 With the original intention of raising monoclonal antibodies to the HIV-1 Gag peptide
108 RMYSPTSIL (RL9HIV) an HIV-1 Gag epitope previously described (Hansen et al., 2016), we
109 immunized human HLA-B27/β2-microglobulin (β2M) transgenic mice (Taurog et al., 1990)
110 (***Figure. S1a-b***) with 293T cells transfected with surface-expressed single-chain HLA-E-RL9HIV
111 complexes (Yu et al., 2002) (***Figure. S1c-d***). We produced hybridomas, and screened culture
112 supernatants for binding on a panel of 293T cells transfected with either single-chain HLA-E-
113 RL9HIV peptide complexes, or with single-chain HLA-E-VL9 peptide complexes as a control.
114 Unexpectedly, we isolated a subset of antibodies that specifically reacted with HLA-E-VL9
115 peptide, the most potent of which was the IgM mAb 3H4. Unlike the well-characterized pan-
116 HLA-E mAb 3D12 (Marin et al., 2003), 3H4 reacted specifically with HLA-E-VL9 (VMAPRTLVL)
117 and not with control, non-VL9 HLA-E-peptide complexes (***Figure. 1a***). Mab 3H4 also bound to

118 VL9 peptide-pulsed HLA-class I negative K562 cells transfected with HLA-E (Lampen et al.,
119 2013) (***Figure. 1b***) and also to soluble HLA-E refolded with synthetic VL9 peptide in both ELISA
120 (***Figure. 1c***) and surface plasmon resonance (SPR) assays (***Figure. 1d***). SPR measurents
121 showed that the 1:1 dissociation constants (K_Ds) of IgM 3H4 and human IgG1 backbone 3H4
122 for soluble HLA-E-VL9 were 8.1 and 49.8 μM, respectively (***Figure. S1e***).
123 Sequence analysis of 3H4 mAb revealed 1.04% heavy chain variable region (V_H) and
124 2.51% light chain viable region (V_L) mutations *(**Table S1**).* We isolated 3 additional HLA-E-VL9
125 mouse mAbs from two additional immunization studies in mice (see Methods), and each of the
126 four HLA-E-VL9 antibodies were minimally mutated IgMs (mean VH and VL mutations, 1.21%
127 and 2.87%, respectively (***Table S1***). Negative stain electron microscopy showed that the 3H4
128 IgM hybridoma antibody was predominantly pentameric with a small proportion of hexamers
129 (***Figure. S1f-g***). In addition, 3H4 was not autoreactive in anti-nuclear antibody or clinical
130 autoantibody assays (***Figure. S1h-i***).
131
132 **3H4 IgM recognized the α1/α2 domain of HLA-E and N-terminus of the VL9 peptide**
133 To map the epitope on the HLA-E-VL9 complex recognized by 3H4, we tested 3H4 binding
134 to VL9 peptide presented by HLA-E, the rhesus ortholog Mamu-E, as well as two HLA-E/Mamu-
135 E hybrids – one with HLA-E α1/Mamu-E α2 (Hα1/Mα2), the other with Mamu-E α1/HLA-E α2
136 (Mα1/Hα2). 3H4 did not bind to Mamu-E/VL9 or Hα1/Mα2-VL9, and its staining of cells
137 expressing Mα1/Hα2-VL9 was weak (***Figure. 1e***), suggesting that 3H4 recognition involved
138 interaction with both α1 and α2 domains of HLA-E, and the epitope on α2 might be partially
139 conserved between human and rhesus. 3H4 also did not cross-react with mouse ortholog Qa-1b
140 (***Figure. S1j***). Moreover, VL9 mutations indicated that position 1 (P1) of the peptide was
141 important for 3H4 binding (***Figure. 1f***), with strong antibody recognition of VL9 peptide P1
142 variants with alanine, cysteine, isoleucine, serine, threonine, weak binding to histidine and
143 proline substitutions, but no interaction with arginine, glutamate, glycine, lysine, methionine,

144 asparagine, tryptophan, tyrosine or phenylalanine (***Figure. 1g and S1k***). These data suggested
145 that mAb 3H4 made contacts with both the HLA-E α1/α2 domain and the amino-terminal end of
146 the VL9 peptide.
147
148 **Co-complex crystal structure of a 3H4 Fab bound to HLA-E-VL9**
149 A co-complex structure of 3H4 Fab bound to HLA-E-VL9, which packed in the C2 space
150 group and diffracted to 1.8 Å (***Table S2a***), was obtained. One of the two copies present in the
151 asymmetric unit is discussed here. 3H4 docked onto the N-terminal region of the HLA-E-
152 peptide-binding groove making contacts with both the heavy chain α-helices in addition to VL9
153 peptide residues 1-4 (***Figure. 2a-b***). The 3H4-HLA-E interface mainly comprised electrostatic
154 interactions and was dominated by the 3H4 VH chain which created a total buried surface area
155 (BSA) of 1109.4 $Å^2$ and formed ten hydrogen bonds (H-bonds) and three salt bridges with HLA-
156 E α1-helix residues and one H-bond with T163 of the HLA-E α2-helix. The smaller 3H4 VL
157 chain-HLA-E interface buried 522.8 $Å^2$ and involved only three inter-molecular H-bonds and
158 three salt bridges (***Tables S2d-h***). Superposition of the 3H4-HLA-E-VL9 co-complex with a
159 published HLA-E-bound CD94/NKG2A structure (Kaiser et al., 2008; Petrie et al., 2008)
160 revealed steric clashes between the VH and VL domains of 3H4 and the CD94 and NKG2A
161 subdomains, respectively (***Figure. 2c-d***). Moreover, seven HLA-E heavy chain residues (α1
162 helix positions 58, 59, 62, 63 and α2 helix positions 162, 163 and 167) are shared 3H4-HLA-E
163 and CD94/NKG2A-HLA-E footprints (***Figure. 2E-F***). Consequently, simultaneous docking of
164 these two HLA-E binding partners, 3H4 and NKG2A/CD94, would likely be disallowed.
165 All four 3H4-derived residues that interfaced with the VL9 peptide (Y97, S100, S100A and
166 Y100B) resided within the VH CDR3 D-junction and were germline-encoded. This 3H4-VL9
167 interface was characterized by weak Van der Waals and hydrophobic contacts, for example,
168 Y100B (3H4) and V1 or P4 (VL9) (***Figure. 2g***). Further, positioning of the Y100B (3H4) side
169 chain directly above V1 (VL9) in part explained preference for small side chains at this peptide

170 position and the dramatic reductions in 3H4 binding to VL9 variants with larger H or F residues
171 at position 1 (***Figure. 1g***). Unique shape complementarity also featured at this interface with the
172 side chains of S100 and S100A (3H4) wrapping around the cyclic side chain of P4 (VL9).
173 The germline-encoded VH CDR3 D-junction residues that formed the 3H4-VL9 interface
174 (Y97, S100, S100A and Y100B), also mediated key HLA-E heavy chain contacts. The surface
175 loop residues A93-V102 swept across the HLA-E-peptide-binding groove forming H-bonds with
176 both the α1 and α2 helices; HLA-E α2 helix T163 formed an H-bond with S100 (3H4), and HLA-
177 E α1-helix R62 formed two H-bonds with the Y100B (3H4) mainchain and an additional H-bond
178 with the main chain of S100A (3H4) (***Figure. 2h***). Y100B (3H4) was involved in multiple polar pi
179 stacking interactions. Not only was the Y100B side chain sandwiched between R62 and W167
180 of the HLA-E α1 and α2 helices, respectively, R62 (HLA-E α1) was also positioned between the
181 aromatic rings of the VH CDR3 domain Y100B and W100D residues.
182 Key contacts outside the germline-encoded CDR3 D-junction region were also formed at
183 the 3H4 VH- and VL-HLA-E interfaces. For 3H4 HC, the VH CDR2 region (residues I51-T57)
184 was positioned above the HLA-E α1-helix where numerous inter-molecular H-bonds were
185 formed involving VH CDR2 residues G56 and N54 in addition to D50, Q61 and K64 of the VH
186 framework region (***Figure. 2h***). Critically, HLA-E α1-helix R65 residue formed four H-bonds with
187 the 3H4 VH and also mediated polar pi stacking interactions with W100D of the VH CDR3 loop.
188 For 3H4 LC, D92 and E93 of the VL CDR3 loop H-bond with K170 of the HLA-E α2-helix and
189 N30 of the VL CDR1 loop formed an H-bond with the α2-helix residue, E166, of HLA-E (***Figure.***
190 ***2i***). Notably, the four key interfacing residues of the 3H4 VH CDR3 D-junction (Y97, S100,
191 S100A and Y100B) were germline-encoded (***Figure. 2j***).
192
193 **3H4 IgM enhanced NK cell cytotoxicity against HLA-E-VL9-expressing target cells**
194 Given the suppressive role of the HLA-E-VL9/NKG2A/CD94 pathway in NK cell function, we
195 tested whether the binding of mAb 3H4 to HLA-E-VL9 could enhance NK cell killing of target

196 cells (***Figure. 3a***). An NKG2A/CD94-positive, CD16/CD32/CD64-negative human NK cell line,
197 NK92 (***Figure. S2a-b***), exhibited significantly increased cytotoxicity against HLA-E-VL9-
198 transfected 293T cells (***Figure. 3b****; P<0.0001,* mixed effects models) but not against non-HLA-
199 E-expressing 293T cells (***Figure. 3c***) in the presence of 3H4 IgM compared to an isotype
200 control IgM. In addition, we tested a combination of 3H4 with the NKG2A specific murine
201 antibody, Z199. While Z199 alone enhanced NK killing against HLA-E-VL9 expressing cells, no
202 additional elevation of killing was observed with the combination of mAbs 3H4 and Z199
203 (***Figure. 3d-e***), suggesting that killing enhancement was maximal with either 3H4 or Z199 alone.
204 These data demonstrated that HLA-E-VL9-specific IgM mAb 3H4 could enhance the killing
205 capacity of NKG2A+ NK cells *in vitro* by binding to HLA-E-VL9 on target cells.
206 The majority of multimeric IgM is restricted to serum and lymph and does not penetrate well
207 into tissues (Sathe and Cusick, 2021). Therefore, we constructed a recombinant 3H4 IgG in a
208 human IgG1 backbone and tested it for ability to enhance NK92 cell killing of HLA-E-VL9 target
209 cells. In contrast to 3H4 IgM, 3H4 IgG could not mediate enhancement of NK cell killing (***Figure.***
210 ***S3a***). Thus, either the affinity of the 3H4 Fab on an IgG was too low (K_D = 49.8 μM; ***Figure.***
211 ***S1e***), or a multimeric antibody is needed for for efficient blocking of HLA-E-VL9 binding to
212 NKG2A/CD94 to enhance of NK killing.
213 To distinguish between the need for higher affinity versus multimerization of the IgM
214 antibody for enhanced NK killing activity, we developed and analyzed 3H4 antibody libraries
215 using high-throughput screening on the surface of yeast (***Figure. 4a***). A library was built that
216 contained ~1.1 million 3H4 scFv variants with amino acid diversity at sites that were determined
217 by structural analysis to interact with HLA-E-VL9 (***Figure. 4b***). Seventeen total residues located
218 in the CDR loops of 3H4 were randomized in groups of four based on their proximity, and all
219 possible combinations of amino acids were sampled at these sites (***Figure. S3b***). The resulting
220 3H4 scFv library was transformed into yeast and screened for three rounds by fluorescence-
221 activated cell sorting (FACS) for binding to fluorescently labeled HLA-E-VL9 tetramer (***Figure.***

222 ***4c***). Eleven 3H4 variants were selected for experimental characterization as recombinant
223 human IgGs from the highly represented clones remaining in the library upon the final selection
224 round. These novel Abs (3H4 Gv1 to 3H4 Gv12) were mutated at positions 97-100 of the CDR
225 H3 loop. Compared to the original 3H4 mAb, the optimized antibodies predominantly contained
226 small amino acids at positions 97 and 98, a polar amino acid at position 99, and a large
227 aromatic at position 100 that is closest to the HLA-E-VL9 (***Figure. 4d***).
228 We next expressed all eleven 3H4 Gv antibodies recombinantnly as human IgGs, and
229 confirmed that they had higher binding than wild-type 3H4 IgG on cell surface expressed HLA-
230 E-VL9 (***Figure. 4e and S3c***). Two 3H4 variants, 3H4 G3v and 3H4 G6v, were selected for
231 affinity and functional analysis. SPR measurents showed that the 1:1 dissociation constants
232 (K_Ds) of the selected 3H4 variants for soluble HLA-E-VL9 were markedly improved compared to
233 that of wild-type 3H4 that had a K_D of 49.8 μM. 3H4 G3v showed the tightest HLA-E-VL9
234 binding, with a K_D of 220 nM, representing a ~226-fold improvement in affinity over the WT mAb
235 (***Figure. 4f***). In the NK cytotoxicity assay, the optimized 3H4 mAbs enhanced NK-92 cell killing
236 of HLA-E-VL9-transfected 293T cells at concentrations of 10 μg/ml and 1 μg/ml to levels
237 comparable to those observed for 3H4 IgM (***Figure. 4g and S3d***). Therefore, the higher affinity
238 of affinity-optimized 3H4 IgG for HLA-E-VL9 could compensate for the need for avidity effect of
239 3H4 IgM multimers to mediate *in vitro* NK enhancement.
240
241 **Isolation of near-germline HLA-E-VL9-specific antibodies from CMV-negative, healthy**
242 **humans**
243 We next asked if similar HLA-E-VL9 antibodies were present in the naïve B cell receptor
244 (BCR) repertoire in humans and whether they could enhance NK killing of target cells. Using
245 HLA-E-VL9 tetramers as probes, we identified B cells expressing HLA-E-VL9-specific B cell
246 receptors (BCRs) in four male, cytomegalovirus (CMV) seronegative human donors (***Figure. 5a***
247 ***and S4a, Table S3***). We isolated 56 HLA-E-VL9-specific antibodies that reacted with HLA-E-

248 VL9 complexes but not control HLA-E-peptide complexes (***Figure. 5b and S4b-c, Table S4***); all
249 were IgM (***Table S4***). By performing more in-depth analysis of the binding profiles of four
250 representative HLA-E-VL9 antibodies - CA123, CA133, CA143 and CA147, we found that these
251 antibodies exhibited differential cross-reactivities with rhesus Mamu-E-VL9 or mouse Qa-1-VL9
252 complexes (***Figure. S4d***) in addition to distinct binding specificities to VL9 peptide variants
253 (***Figure. S4e***) . The apparent affinities (K_D) of CA123 and CA147 on a human IgG1 backbone to
254 soluble HLA-E-VL9 were 3.8 and 25.0 μM, respectively (***Figure. S4f***). Human HLA-E-VL9
255 antibodies CA147 and CA123 tested in functional NK killing assays as a recombinant human
256 IgG1. CA147 enhanced NK-92 cell cytotoxicity to HLA-E-VL9-expressing target cells (***Figure.***
257 ***5c***), whereas CA123 had no enhancing effect (***Figure. S4g-h***), suggesting that NK killing-
258 enhancement function of the HLA-E-VL9 antibodies was determined by factors beyond binding
259 affinity.
260 In the four humans, the percentages of HLA-E-VL9-specific B cells in pan-B cells ($CD3^-$
261 $CD235^-CD14^-CD16^-CD19^+$) were 0.0009%-0.0023% (mean of 0.0014%) (***Figure. 5d***). HLA-E-
262 VL9-specific B cells were $IgD^+IgM^{+/-}$ B cells, in which four cell subsets were observed (***Figure.***
263 ***5e***) – $CD10^-CD27^-CD38^{+/-}$ naïve B cells (71.4%), $CD10^+CD27^-CD38^{++}$ immature or newly formed
264 B cells (Giltiay et al., 2019) (10.7%), and $CD10^-CD27^+CD38^-$ non-class-switched memory cells,
265 demonstrating that BCRs targeting HLA-E-VL9 peptide existed in the naïve B cell repertoire of
266 healthy humans.
267
268 **V_H/V_L gene usage of HLA-E-VL9-specific antibodies**
269 To characterize the human antibody gene usage of HLA-E-VL9 antibodies, we analyzed the
270 paired heavy chain and light chain gene sequences of 56 human HLA-E-VL9 antibodies, and
271 found 1 multiple-member clone containing 6 antibodies in donor LP021 (Kepler et al., 2014)
272 (***Table S4***). Next, we compared the 51 HLA-E-VL9-specific B cell clones with a reference
273 human antibody repertoire (DeKosky et al., 2015). Over 45% of the heavy chain variable region

274 (V_H) genes were VH3-21 or VH3-11 in HLA-E-VL9 antibodies, whereas less than 7% of the
275 control B cells used these two genes (***Figure. 5f, Table S4***). HLA-E-VL9 antibody light chain
276 variable regions (V_κ/V_λ) also were skewed and preferentially utilized IGKV3-15, IGKV1-39 and
277 IGKV3-11 genes compared to controls (***Figure. 5g, Table S4***). No J chain gene usage
278 preference was observed (***Figure. S5a-d***). Moreover, HLA-E-VL9 antibodies showed a trend to
279 have shorter heavy chain complementarity determining region 3 (CDR3) lengths than reference
280 antibodies (***Figure. 5h***), while no difference was observed for light chain CDR3 (***Figure. 5i***).
281 Given that HLA-E-VL9 antibodies were IgMs derived primarily from naïve or immature B cells,
282 we compared the mutation frequencies of the 51 clones with a reference human antibody
283 repertoire containing both naïve and antigen-experienced antibodies (DeKosky et al., 2016).
284 Both HLA-E-VL9 antibody heavy and light chain variable region genes exhibited low somatic
285 mutation rates that were similar to naïve B cell controls (***Figure. 5j-k***). Thus, human HLA-E-
286 VL9-specific antibodies were IgM, minimally mutated and displayed skewed usage of V_H and
287 V_κ/V_λ genes.
288

289 **DISCUSSION**

290 In this study, we have isolated and characterized antibodies reactive with HLA-E-VL9
291 peptide complexes, and found these antibodies were derived from the naïve IgM B cell BCR
292 repertoire in mice as well as in human blood donors. We selected HCMV negative donors to
293 avoid possible cross reacting antibody responses to the VL9 sequence present in the signal
294 peptide of the UL40 protein, and male donors to exclude anti-HLA antibodies made in
295 pregnancy. Somatic mutations of these antibodies were minimal, and the affinities of these
296 antibodies for HLA-E-VL9 were low. The lack of class-switching in HLA-E-VL9-specific
297 antibodies may reflect self-tolerance of CD4 T cells and a lack of T cell help for affinity
298 maturation of these antibodies. While the mouse antibodies were selected in the setting of HLA-
299 E-unrelated peptide immunizations, they were minimally mutated IgM antibodies, as were the

300 antibodies isolated from human CMV-negative, healthy males. Structural analysis of the HLA-E-
301 VL9-3H4 Fab co-complex revealed that the murine 3H4 heavy chain made key contacts with
302 HLA-E and the VL9 peptide using germline-encoded residues in the CDR-H3 (D) region.
303 However, 3H4 is a mouse antibody that reacted with human HLA-E-VL9. The HLA-E equivalent
304 in C57BL/6xSJL mice is Qa1b which presents a similar class Ia signal peptide AMAPRTLLL but
305 3H4 did not bind to this HLA-E-peptide complex. Therefore, it remains unclear how 3H4 and
306 possibly the other HLA-E-VL9-specific IgM antibodies were genetically selected as germlines or
307 induced with minimal mutation in the setting of HLA-E-unrelated peptide immunizations. In
308 contrast, the human antibodies such as CA147 that bound to human HLA-E-VL9 were auto-
309 antibodies with near germline sequences that exist in some, possibly many, individuals.
310 Autoantibodies to HLA-Ia (Alberu et al., 2007; Morales-Buenrostro et al., 2008) and HLA-E
311 heavy chains (Ravindranath et al., 2010a; Ravindranath et al., 2010b) have been detected in
312 non-alloimmunized males, and can contribute to allograft damage (Hickey et al., 2016;
313 McKenna et al., 2000). It has been suggested that the HLA-E antibodies in non-alloimmunized
314 humans could be elicited by autoantigens derived from soluble HLA-E heavy chains that
315 become immunogenic without the β2M subunit, or viral/bacterial agents cross-reactive with
316 HLAs (Alberu et al., 2007; Hickey et al., 2016; Ravindranath et al., 2010a; Ravindranath et al.,
317 2010b). It is of interest that human cytomegalovirus (CMV), which encodes the VL9 sequence
318 VMAPRTLIL in the leader sequence of its UL40 gene. This peptide is processed in a TAP
319 independent manner and presented bound to HLA-E at the cell surface to inhibit NK cell killing
320 and evade innate immune responses (Tomasec et al., 2000). This has not been reported to
321 elicit antibody responses, but HLA-E-UL40 peptide-specific T cells have been described when
322 the limited polymorphism in the HLA A, B and C sequences mismatches that of the virally-
323 encoded VL9 peptide sufficiently to overcome self-tolerance (Sullivan et al., 2015). However,
324 the subjects in our study were all HCMV seronegative and male. The possibility that germline

325 encoded anti-HLA-E-VL9 antibodies play a physiological role in regulating NK cell function in
326 several species needs further exploration.
327 Harnessing NK cells to attack tumor cells has emerged as an attractive strategy for cancer
328 immunotherapies (Guillerey et al., 2016; Lowry and Zehring, 2017). A promising target for
329 therapeutic immune-modulation of NK cell functions is the inhibitory NKG2A/CD94-HLA-E-VL9
330 interaction. Monalizumab, the first-in-class monoclonal antibody checkpoint inhibitor targeting
331 NKG2A, enhances anti-tumor immunity by activating cytotoxic activities of effector CD8+ T cells
332 and NK cells (Andre et al., 2018; Creelan and Antonia, 2019; van Hall et al., 2019). In our study,
333 co-complex structural analysis revealed steric clashes between the 3H4 Fab and the NK
334 inhibitory receptor NKG2A/CD94 when docked onto HLA-E-VL9, showing how 3H4 IgM can
335 enhance NKG2A+ NK cell killing. Both mouse 3H4 IgM, the affinity-optimized 3H4 IgG, and the
336 recombinant IgG1 form of human CA147 enhanced the cytotoxicity of an NKG2A+ human NK
337 cell line NK92, which is a safe and established cell line that has been used for adoptive
338 immunotherapy in phase I clinical trials (Klingemann et al., 2016). Thus, HLA-E-VL9-targeting
339 antibodies 3H4 and CA147 could have therapeutic potential as NK checkpoint inhibitors.
340
341 **METHODS**
342 Detailed methods are provided in the supplemental online material.
343
344 **ACKNOWLEDGMENTS**
345 We thank Duke Human Vaccine Institute (DHVI) programs and finance staff for project
346 oversight and the contributions of technical staff at the DHVI, including Jordan Cocchiaro, Kelly
347 Soderberg, Ahmed Yousef Abuahmad, Yunfei Wang, Giovanna Hernandez, Esther Lee, Paige
348 Power, Aja Sanzone, Brenna Harrington, Andrew Foulger, Amanda Newman, Cindy Bowman,
349 Grace Stevens, Laura Sutherland, Margaret Deyton, Victoria Gee-Lai, Tarra Von Holle, Thad
350 Gurley, Madison Berry, Kara Anasti, Katayoun Mansouri, Erika Dunford, and Dawn Jones

Marshall. We thank the DHVI Flow Cytometry Core and Duke Cancer Institute Flow Cytometry Shared Resource (FCSR) for technical assistance. This study was funded by the Collaboratory of AIDS Researchers for Eradication (CARE; UM1AI126619) (B.F.H.) and the Bill and Melinda Gates Foundation OPP1108533 (A.J.M.). P.B and A.J.M. are Jenner Institute Investigators.

ACCESSION NUMBERS

The 3H4-HLA-E-VL9 co-complex structure determined in this study has the PDB accession code, 7BH8.

AUTHOR CONTRIBUTIONS

D.L. isolated and characterized antibodies, performed ^{51}Cr release assay, and analyzed data. S.B. made single-chain trimer constructs, performed epitope mapping experiments and analyzed data. G.M.G, L.W. and M.Q. prepared the antigens and HLA-E tetramers. L.W., G.M.G., D.R. and K.H performed structural experiments with oversight from E.Y.J.. O.S. and M.L.A. performed antibody affinity optimization work. D.W.C. helped with flow cytometry sorting set-up. R.S., R.P. and M.B. performed hybridoma experiments, ELISA assays and help with ^{51}Cr release assays. R.J.E. oversaw negative stain EM. M.A. supervised and interpreted the SPR experiments. K.W. oversaw and performed antibody gene sequence analysis. Z.M. and M.B. helped with antibody isolation. Y.W. and W.R. provided statistical analysis. K.O.S. oversaw antigen production. G.F. and P.B. provided advice on NK cell assays and contributed to study design and data interpretation. B.F.H. and A.J.M. conceived, designed, coordinated the study. D.L. and B.F.H. wrote the manuscript, which was edited by L.W., S.B., O.S., M.L.A., P.B., G.M.G., and A.J.M., and reviewed by all authors.

DECLARATION OF INTERESTS

D.L., S.B., M.L.A., G.M.G., A.J.M. and B.F.H. have patents submitted on antibodies and select methods in this paper.

REFERENCES

Alberu, J., Morales-Buenrostro, L.E., de Leo, C., Vargas-Rojas, M.I., Marino-Vazquez, L.A., and Crispin, J.C. (2007). A non-allogeneic stimulus triggers the production of de novo HLA antibodies in healthy adults. Transpl Immunol *18*, 166-171.

Aldrich, C.J., DeCloux, A., Woods, A.S., Cotter, R.J., Soloski, M.J., and Forman, J. (1994). Identification of a Tap-dependent leader peptide recognized by alloreactive T cells specific for a class Ib antigen. Cell *79*, 649-658.

Andre, P., Brunet, C., Guia, S., Gallais, H., Sampol, J., Vivier, E., and Dignat-George, F. (1999). Differential regulation of killer cell Ig-like receptors and CD94 lectin-like dimers on NK and T lymphocytes from HIV-1-infected individuals. Eur J Immunol *29*, 1076-1085.

Andre, P., Denis, C., Soulas, C., Bourbon-Caillet, C., Lopez, J., Arnoux, T., Blery, M., Bonnafous, C., Gauthier, L., Morel, A.*, et al.* (2018). Anti-NKG2A mAb Is a Checkpoint Inhibitor that Promotes Anti-tumor Immunity by Unleashing Both T and NK Cells. Cell *175*, 1731-1743 e1713.

Braud, V., Jones, E.Y., and McMichael, A. (1997). The human major histocompatibility complex class Ib molecule HLA-E binds signal sequence-derived peptides with primary anchor residues at positions 2 and 9. Eur J Immunol *27*, 1164-1169.

Braud, V.M., Allan, D.S., O'Callaghan, C.A., Soderstrom, K., D'Andrea, A., Ogg, G.S., Lazetic, S., Young, N.T., Bell, J.I., Phillips, J.H.*, et al.* (1998). HLA-E binds to natural killer cell receptors CD94/NKG2A, B and C. Nature *391*, 795-799.

Brooks, A.G., Posch, P.E., Scorzelli, C.J., Borrego, F., and Coligan, J.E. (1997). NKG2A complexed with CD94 defines a novel inhibitory natural killer cell receptor. J Exp Med *185*, 795-800.

402 Chiossone, L., Dumas, P.Y., Vienne, M., and Vivier, E. (2018). Natural killer cells and other
403 innate lymphoid cells in cancer. Nat Rev Immunol *18*, 671-688.
404 Colonna, M., and Samaridis, J. (1995). Cloning of immunoglobulin-superfamily members
405 associated with HLA-C and HLA-B recognition by human natural killer cells. Science *268*, 405-
406 408.
407 Creelan, B.C., and Antonia, S.J. (2019). The NKG2A immune checkpoint - a new direction in
408 cancer immunotherapy. Nat Rev Clin Oncol *16*, 277-278.
409 DeKosky, B.J., Kojima, T., Rodin, A., Charab, W., Ippolito, G.C., Ellington, A.D., and Georgiou,
410 G. (2015). In-depth determination and analysis of the human paired heavy- and light-chain
411 antibody repertoire. Nat Med *21*, 86-91.
412 DeKosky, B.J., Lungu, O.I., Park, D., Johnson, E.L., Charab, W., Chrysostomou, C., Kuroda, D.,
413 Ellington, A.D., Ippolito, G.C., Gray, J.J.*, et al.* (2016). Large-scale sequence and structural
414 comparisons of human naive and antigen-experienced antibody repertoires. Proc Natl Acad Sci
415 U S A *113*, E2636-2645.
416 Giltiay, N.V., Giordano, D., and Clark, E.A. (2019). The Plasticity of Newly Formed B Cells. J
417 Immunol *203*, 3095-3104.
418 Guillerey, C., Huntington, N.D., and Smyth, M.J. (2016). Targeting natural killer cells in cancer
419 immunotherapy. Nat Immunol *17*, 1025-1036.
420 Hansen, S.G., Wu, H.L., Burwitz, B.J., Hughes, C.M., Hammond, K.B., Ventura, A.B., Reed,
421 J.S., Gilbride, R.M., Ainslie, E., Morrow, D.W.*, et al.* (2016). Broadly targeted CD8(+) T cell
422 responses restricted by major histocompatibility complex E. Science *351*, 714-720.
423 Hickey, M.J., Valenzuela, N.M., and Reed, E.F. (2016). Alloantibody Generation and Effector
424 Function Following Sensitization to Human Leukocyte Antigen. Front Immunol *7*, 30.
425 Hu, W., Wang, G., Huang, D., Sui, M., and Xu, Y. (2019). Cancer Immunotherapy Based on
426 Natural Killer Cells: Current Progress and New Opportunities. Front Immunol *10*, 1205.

427 Joosten, S.A., van Meijgaarden, K.E., van Weeren, P.C., Kazi, F., Geluk, A., Savage, N.D.,
428 Drijfhout, J.W., Flower, D.R., Hanekom, W.A., Klein, M.R.*, et al.* (2010). Mycobacterium
429 tuberculosis peptides presented by HLA-E molecules are targets for human CD8 T-cells with
430 cytotoxic as well as regulatory activity. PLoS Pathog *6*, e1000782.
431 Kaiser, B.K., Pizarro, J.C., Kerns, J., and Strong, R.K. (2008). Structural basis for NKG2A/CD94
432 recognition of HLA-E. Proc Natl Acad Sci U S A *105*, 6696-6701.
433 Karlhofer, F.M., Ribaudo, R.K., and Yokoyama, W.M. (1992). MHC class I alloantigen specificity
434 of Ly-49+ IL-2-activated natural killer cells. Nature *358*, 66-70.
435 Kepler, T.B., Munshaw, S., Wiehe, K., Zhang, R., Yu, J.S., Woods, C.W., Denny, T.N.,
436 Tomaras, G.D., Alam, S.M., Moody, M.A.*, et al.* (2014). Reconstructing a B-Cell Clonal Lineage.
437 II. Mutation, Selection, and Affinity Maturation. Front Immunol *5*, 170.
438 Kim, N., Lee, H.H., Lee, H.J., Choi, W.S., Lee, J., and Kim, H.S. (2019). Natural killer cells as a
439 promising therapeutic target for cancer immunotherapy. Arch Pharm Res *42*, 591-606.
440 Klingemann, H., Boissel, L., and Toneguzzo, F. (2016). Natural Killer Cells for Immunotherapy -
441 Advantages of the NK-92 Cell Line over Blood NK Cells. Front Immunol *7*, 91.
442 Kraemer, T., Blasczyk, R., and Bade-Doeding, C. (2014). HLA-E: a novel player for
443 histocompatibility. J Immunol Res *2014*, 352160.
444 Kraemer, T., Celik, A.A., Huyton, T., Kunze-Schumacher, H., Blasczyk, R., and Bade-Doding, C.
445 (2015). HLA-E: Presentation of a Broader Peptide Repertoire Impacts the Cellular Immune
446 Response-Implications on HSCT Outcome. Stem Cells Int *2015*, 346714.
447 Lampen, M.H., Hassan, C., Sluijter, M., Geluk, A., Dijkman, K., Tjon, J.M., de Ru, A.H., van der
448 Burg, S.H., van Veelen, P.A., and van Hall, T. (2013). Alternative peptide repertoire of HLA-E
449 reveals a binding motif that is strikingly similar to HLA-A2. Mol Immunol *53*, 126-131.
450 Lee, N., Goodlett, D.R., Ishitani, A., Marquardt, H., and Geraghty, D.E. (1998a). HLA-E surface
451 expression depends on binding of TAP-dependent peptides derived from certain HLA class I
452 signal sequences. J Immunol *160*, 4951-4960.

453 Lee, N., Llano, M., Carretero, M., Ishitani, A., Navarro, F., Lopez-Botet, M., and Geraghty, D.E.
454 (1998b). HLA-E is a major ligand for the natural killer inhibitory receptor CD94/NKG2A. Proc
455 Natl Acad Sci U S A *95*, 5199-5204.
456 Ljunggren, H.G., and Karre, K. (1985). Host resistance directed selectively against H-2-deficient
457 lymphoma variants. Analysis of the mechanism. J Exp Med *162*, 1745-1759.
458 Ljunggren, H.G., and Karre, K. (1990). In search of the 'missing self': MHC molecules and NK
459 cell recognition. Immunol Today *11*, 237-244.
460 Llano, M., Lee, N., Navarro, F., Garcia, P., Albar, J.P., Geraghty, D.E., and Lopez-Botet, M.
461 (1998). HLA-E-bound peptides influence recognition by inhibitory and triggering CD94/NKG2
462 receptors: preferential response to an HLA-G-derived nonamer. Eur J Immunol *28*, 2854-2863.
463 Lowry, L.E., and Zehring, W.A. (2017). Potentiation of Natural Killer Cells for Cancer
464 Immunotherapy: A Review of Literature. Front Immunol *8*, 1061.
465 Mahapatra, S., Mace, E.M., Minard, C.G., Forbes, L.R., Vargas-Hernandez, A., Duryea, T.K.,
466 Makedonas, G., Banerjee, P.P., Shearer, W.T., and Orange, J.S. (2017). High-resolution
467 phenotyping identifies NK cell subsets that distinguish healthy children from adults. PLoS One
468 *12*, e0181134.
469 Marin, R., Ruiz-Cabello, F., Pedrinaci, S., Mendez, R., Jimenez, P., Geraghty, D.E., and
470 Garrido, F. (2003). Analysis of HLA-E expression in human tumors. Immunogenetics *54*, 767-
471 775.
472 McKenna, R.M., Takemoto, S.K., and Terasaki, P.I. (2000). Anti-HLA antibodies after solid
473 organ transplantation. Transplantation *69*, 319-326.
474 McMurtrey, C., Harriff, M.J., Swarbrick, G.M., Duncan, A., Cansler, M., Null, M., Bardet, W.,
475 Jackson, K.W., Lewinsohn, D.A., Hildebrand, W.*, et al.* (2017). T cell recognition of
476 Mycobacterium tuberculosis peptides presented by HLA-E derived from infected human cells.
477 PLoS One *12*, e0188288.

478 Michaelsson, J., Teixeira de Matos, C., Achour, A., Lanier, L.L., Karre, K., and Soderstrom, K.
479 (2002). A signal peptide derived from hsp60 binds HLA-E and interferes with CD94/NKG2A
480 recognition. J Exp Med *196*, 1403-1414.
481 Morales-Buenrostro, L.E., Terasaki, P.I., Marino-Vazquez, L.A., Lee, J.H., El-Awar, N., and
482 Alberu, J. (2008). "Natural" human leukocyte antigen antibodies found in nonalloimmunized
483 healthy males. Transplantation *86*, 1111-1115.
484 Pende, D., Falco, M., Vitale, M., Cantoni, C., Vitale, C., Munari, E., Bertaina, A., Moretta, F., Del
485 Zotto, G., Pietra, G.*, et al.* (2019). Killer Ig-Like Receptors (KIRs): Their Role in NK Cell
486 Modulation and Developments Leading to Their Clinical Exploitation. Front Immunol *10*, 1179.
487 Petrie, E.J., Clements, C.S., Lin, J., Sullivan, L.C., Johnson, D., Huyton, T., Heroux, A., Hoare,
488 H.L., Beddoe, T., Reid, H.H.*, et al.* (2008). CD94-NKG2A recognition of human leukocyte
489 antigen (HLA)-E bound to an HLA class I leader sequence. J Exp Med *205*, 725-735.
490 Raulet, D.H. (2006). Missing self recognition and self tolerance of natural killer (NK) cells. Semin
491 Immunol *18*, 145-150.
492 Ravindranath, M.H., Kaneku, H., El-Awar, N., Morales-Buenrostro, L.E., and Terasaki, P.I.
493 (2010a). Antibodies to HLA-E in nonalloimmunized males: pattern of HLA-Ia reactivity of anti-
494 HLA-E-positive sera. J Immunol *185*, 1935-1948.
495 Ravindranath, M.H., Taniguchi, M., Chen, C.W., Ozawa, M., Kaneku, H., El-Awar, N., Cai, J.,
496 and Terasaki, P.I. (2010b). HLA-E monoclonal antibodies recognize shared peptide sequences
497 on classical HLA class Ia: relevance to human natural HLA antibodies. Mol Immunol *47*, 1121-
498 1131.
499 Rolle, A., Meyer, M., Calderazzo, S., Jager, D., and Momburg, F. (2018). Distinct HLA-E
500 Peptide Complexes Modify Antibody-Driven Effector Functions of Adaptive NK Cells. Cell Rep
501 *24*, 1967-1976 e1964.
502 Sathe, A., and Cusick, J.K. (2021). Biochemistry, Immunoglobulin M. In StatPearls (Treasure
503 Island (FL)).

504 Sensi, M., Pietra, G., Molla, A., Nicolini, G., Vegetti, C., Bersani, I., Millo, E., Weiss, E., Moretta,
505 L., Mingari, M.C.*, et al.* (2009). Peptides with dual binding specificity for HLA-A2 and HLA-E are
506 encoded by alternatively spliced isoforms of the antioxidant enzyme peroxiredoxin 5. Int
507 Immunol *21*, 257-268.
508 Souza-Fonseca-Guimaraes, F., Cursons, J., and Huntington, N.D. (2019). The Emergence of
509 Natural Killer Cells as a Major Target in Cancer Immunotherapy. Trends Immunol *40*, 142-158.
510 Sullivan, L.C., Westall, G.P., Widjaja, J.M., Mifsud, N.A., Nguyen, T.H., Meehan, A.C.,
511 Kotsimbos, T.C., and Brooks, A.G. (2015). The Presence of HLA-E-Restricted, CMV-Specific
512 CD8+ T Cells in the Blood of Lung Transplant Recipients Correlates with Chronic Allograft
513 Rejection. PLoS One *10*, e0135972.
514 Taurog, J., Hammer, R., Maika, S., Sams, K., El-Zaatari, F., Stimpson, S., and Schwab, J.
515 (1990). HLA-B27 transgenic mice as potential models of human disease. In Transgenic mice
516 and mutants in MHC research (Springer), pp. 268-275.
517 Tomasec, P., Braud, V.M., Rickards, C., Powell, M.B., McSharry, B.P., Gadola, S., Cerundolo,
518 V., Borysiewicz, L.K., McMichael, A.J., and Wilkinson, G.W. (2000). Surface expression of HLA-
519 E, an inhibitor of natural killer cells, enhanced by human cytomegalovirus gpUL40. Science *287*,
520 1031.
521 van Hall, T., Andre, P., Horowitz, A., Ruan, D.F., Borst, L., Zerbib, R., Narni-Mancinelli, E., van
522 der Burg, S.H., and Vivier, E. (2019). Monalizumab: inhibiting the novel immune checkpoint
523 NKG2A. J Immunother Cancer *7*, 263.
524 van Meijgaarden, K.E., Haks, M.C., Caccamo, N., Dieli, F., Ottenhoff, T.H., and Joosten, S.A.
525 (2015). Human CD8+ T-cells recognizing peptides from Mycobacterium tuberculosis (Mtb)
526 presented by HLA-E have an unorthodox Th2-like, multifunctional, Mtb inhibitory phenotype and
527 represent a novel human T-cell subset. PLoS Pathog *11*, e1004671.

528 van Montfoort, N., Borst, L., Korrer, M.J., Sluijter, M., Marijt, K.A., Santegoets, S.J., van Ham,
529 V.J., Ehsan, I., Charoentong, P., Andre, P.*, et al.* (2018). NKG2A Blockade Potentiates CD8 T
530 Cell Immunity Induced by Cancer Vaccines. Cell *175*, 1744-1755 e1715.
531 Walters, L.C., Harlos, K., Brackenridge, S., Rozbesky, D., Barrett, J.R., Jain, V., Walter, T.S.,
532 O'Callaghan, C.A., Borrow, P., Toebes, M.*, et al.* (2018). Pathogen-derived HLA-E bound
533 epitopes reveal broad primary anchor pocket tolerability and conformationally malleable peptide
534 binding. Nat Commun *9*, 3137.
535 Yokoyama, W.M., and Kim, S. (2006). How do natural killer cells find self to achieve tolerance?
536 Immunity *24*, 249-257.
537 Yu, Y.Y., Netuschil, N., Lybarger, L., Connolly, J.M., and Hansen, T.H. (2002). Cutting edge:
538 single-chain trimers of MHC class I molecules form stable structures that potently stimulate
539 antigen-specific T cells and B cells. J Immunol *168*, 3145-3149.
540
541

542 **FIGURES**

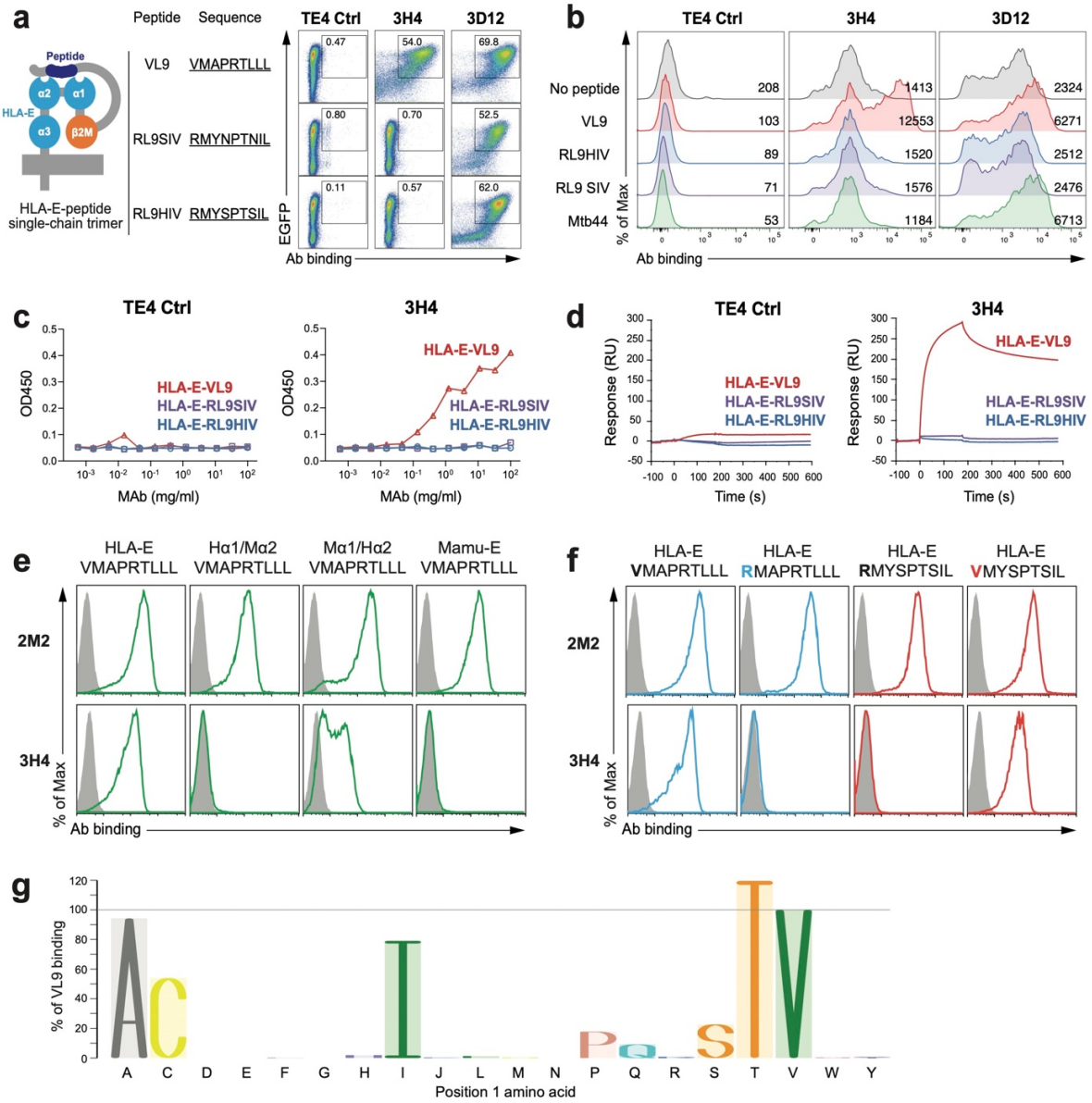

543

544 **Figure. 1 Isolation of monoclonal antibody 3H4 specifically targeting HLA-E-VL9**

545 **complex.**

546 **a, 3H4 bound HLA-E-VL9 single chain trimer (SCT)-transfected 293T cells.** All SCT

547 constructs express EGFP to indicate transfection efficiency. Transfected cells were stained with

548 test antibody and then an Alexa fluor 555 (AF555)-anti-mouse Ig(H+L) secondary antibody. A

549 control mouse IgM TE4 was used as a negative control. Anti-pan-HLA-E antibody 3D12 was
550 used as a positive control. Representative data from one of five independent experiments are
551 shown.
552 **b, 3H4 bound VL9 peptide pulsed K562-HLA-E cells.** RL9HIV, RL9SIV, Mtb44 peptides
553 served as peptide controls. TE4 and 3D12 were used as antibody controls. Peptide-pulsed cells
554 were stained with test antibody and then an Alexa fluor 647 (AF647)-anti-mouse Ig(H+L)
555 secondary antibody. Mean fluorescence intensity (MFI) of each sample is shown.
556 Representative data from one of three independent experiments are shown.
557 **c-d, 3H4 specifically bound to soluble HLA-E-VL9 complexes as measured by ELISA and**
558 **SPR**. **c,** ELISA plates were coated with 3H4 or control IgM TE4 in serial dilution, blocked, and
559 incubated with C-trap-stabilized HLA-E-VL9, HLA-E-RL9HIV, HLA-E-RL9SIV antigens. After
560 washing, antigen binding was detected by adding HRP-conjugated anti-human β2M antibody. **d,**
561 For SPR, biotinylated HLA-E-peptide complexes (HLA-E-VL9, HLA-E-RL9SIV, HLA-E-RL9HIV
562 and mock control) were bound to the immobilized streptavidin. Antibody 3H4 and control TE4
563 were flowed over sensor chips and antibody binding was monitored in real-time. Representative
564 data from one of two independent experiments are shown.
565 **e, 3H4 recognized the α2 domain of HLA-E.** Flow cytometry analysis of 3H4 and 2M2 (a
566 control β2M mAb) binding to 293T cells transfected with VL9 presented by HLA-E, Mamu-E, and
567 two HLA-E/Mamu-E hybrids - one with HLA-E α1/Mamu-E α2 (Hα1/Mα2), the other with Mamu-
568 E α1/HLA-E α2 (Mα1/Hα2) (green). Transfected cells were stained with test antibody and then
569 an AF647-anti-mouse Ig(H+L) secondary antibody. Isotype control stained cells were used as
570 negative controls (grey filled histograms). Representative data from one of three independent
571 experiments are shown.
572 **f, 3H4 recognized position 1 (P1) of the VL9 peptide.** 3H4 and 2M2 (a control β2M mAb)
573 staining of 293T cells transfected with HLA-E-VL9 (VMAPRTLLL) or HLA-E-VL9 with a mutation
574 at P1 (valine to arginine; RMAPRTLLL) (blue), and with HLA-E-RL9HIV (RMYSPTSIL) or HLA-

575 E-RL9HIV with a mutation at P1 (arginine to valine; VMYSPTSIL) (red). Transfected cells were
576 stained with test antibody and then an AF647-anti-mouse Ig(H+L) secondary antibody. Isotype
577 control stained cells were used as negative controls (grey filled histograms). Representative
578 data from one of three independent experiments are shown.
579 **g, 3H4 recognized peptides with variants in P1**. 293T cells were transfected with HLA-E
580 SCTs with VL9 peptides with single amino acid mutations at P1, then stained with 3H4 antibody
581 followed by AF647 conjugated anti-mouse IgG(H+L) secondary antibody. Cells were gated for
582 EGFP positive subsets. MFI of 3H4 staining on wildtype VL9 peptide was set as 100%, and the
583 percentages for binding to mutants calculated as (MFI of 3H4 binding on each P1 variant) / (MFI
584 of 3H4 binding on wildtype VL9) x 100%.
585

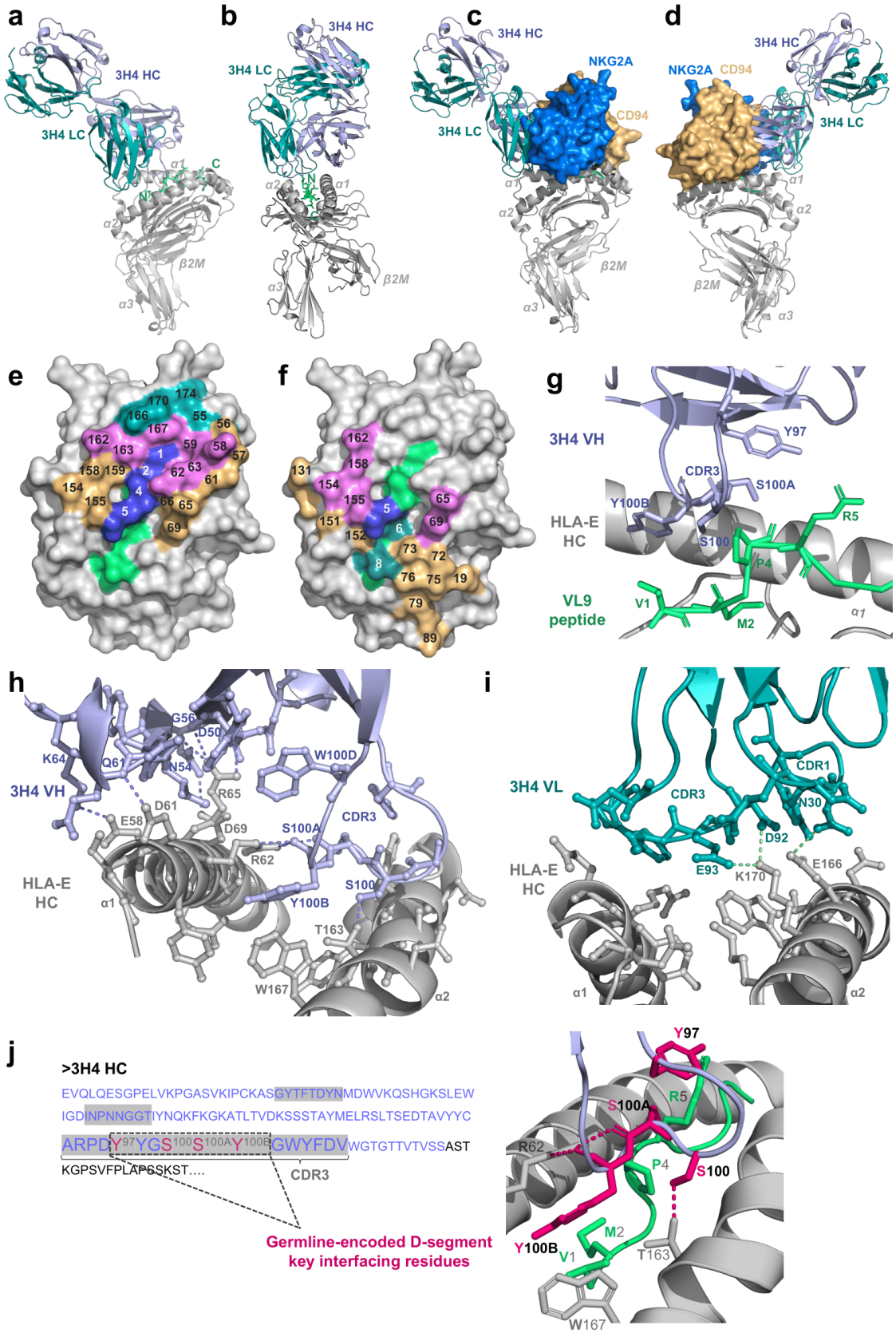
a
3H4 HC
3H4 LC
α1
α2
β2M
α3
b
3H4 HC
3H4 LC
α2
α1
β2M
α3
c
3H4 HC
NKG2A
CD94
3H4 LC
α1
α2
β2M
α3
d
3H4 HC
NKG2A
CD94
3H4 LC
α1
α2
β2M
α3
e
f
g
3H4 VH
Y97
CDR3
S100A
Y100B
HLA-E HC
R5
S100
P4
VL9 peptide
V1
M2
α1
h
G56
D50
K64
Q61
N54
W100D
3H4 VH
R65
D61
E58
D69
S100A
CDR3
R62
HLA-E HC
α1
S100
Y100B
T163
W167
α2
i
3H4 VL
CDR1
CDR3
N30
D92
E93
K170
E166
HLA-E HC
α1
α2
j
>3H4 HC
EVQLQESGPELVKPGASVKIPCKASGYTFTDYNMDWVKQSHGKSLEW
IGDINPNNGGTIYNQKFKGKATLTVDKSSSTAYMELRSLTSEDTAVYYC
ARPDY97YGS100S100AY100BGWYFDVWGTGTTVTVSSAST
KGPSVFPLAPSSKST....
CDR3
Germline-encoded D-segment
key interfacing residues
Y97
R5
S100A
R62
P4
S100
M2
Y100B
V1
T163
W167

586

587 **Figure. 2 3H4 Fab-HLA-E-VL9 co-complex structural visualization**.

588 **a-b, 3H4 Fab-HLA-E docking angles.** HLA-E heavy chain and β2M light chain: grey; VL9
589 peptide: lime green; 3H4 heavy chain: light purple; 3H4 light chain: teal.

590 **c-d, Superposition of 3H4 Fab and CD94/NKG2A docking sites on HLA-E.** The HLA-E
591 complex and 3H4 Fab are color-coded according to A and B. CD94: orange; NKG2A: marine
592 blue.

593 **e, Aerial view of the HLA-E-VL9 peptide binding groove surface.** Non-interfacing HLA-E
594 residues: light grey; non-interfacing peptide residues: lime green; VL9 peptide residues involved
595 in the 3H4 interface: marine blue. Interfacing HLA-E residues that contact 3H4 heavy and light
596 chain: orange and teal, respectively; interfacing HLA-E residues that contact both 3H4 heavy
597 and light chains: violet. Residue positions are numbered on the HLA-E surface view.

598 **f, Aerial view of the overlapping 3H4 and CD94/NKG2A footprints on the HLA-E peptide**
599 **binding groove.** VL9 peptide residues involved in both the 3H4 and CD94/NKG2A interfaces:
600 marine blue; HLA-E heavy chain residues involved in both interfaces: violet. Peptide and HLA-E
601 heavy chain residues involved exclusively in the CD94/NKG2A interface: teal and orange,
602 respectively.

603 **g, Binding interface of 3H4 HC/VL9 peptide.** Interfacing residues (Y97, S100, S100A and
604 Y100B of the VH CDR3 loop and V1, M2, P4 and R5 of the VL9 peptide) are shown in ball and
605 stick-form with non-interfacing residues in cartoon form. VL9 peptide: lime green; HLA-E heavy
606 chain: grey; 3H4 heavy chain: light purple.

607 **h-i, Binding interfaces of 3H4 HC/HLA-E heavy chain (h) and 3H4 LC/HLA-E HC (i).**
608 Interfacing residues are displayed in ball-and-stick form, non-interfacing residues are displayed
609 in cartoon form and hydrogen bonds as dashed lines.

610 **j, Key interfacing residues within the germline-encoded D-junction.** 3H4 heavy chain VH
611 sequence were in purple and the CDR1/2/3 regions shaded grey. Germline-encoded residues
612 within the VH CDR3 D-junction are denoted. The 4 key interfacing residues (Y97, S100, S100A

613 and Y100B) within this germline-encoded D-junction that make contacts both the HLA-E heavy
614 chain and VL9 peptide are highlighted magenta in the sequence and illustrated as magenta
615 sticks in the PyMol visualization. HLA-E heavy chain: grey; VL9 peptide: green; hydrogen
616 bonds: magenta dashed lines; residues of the 3H4 heavy chain that are not germline-encoded
617 key interfacing residues: light purple.
618

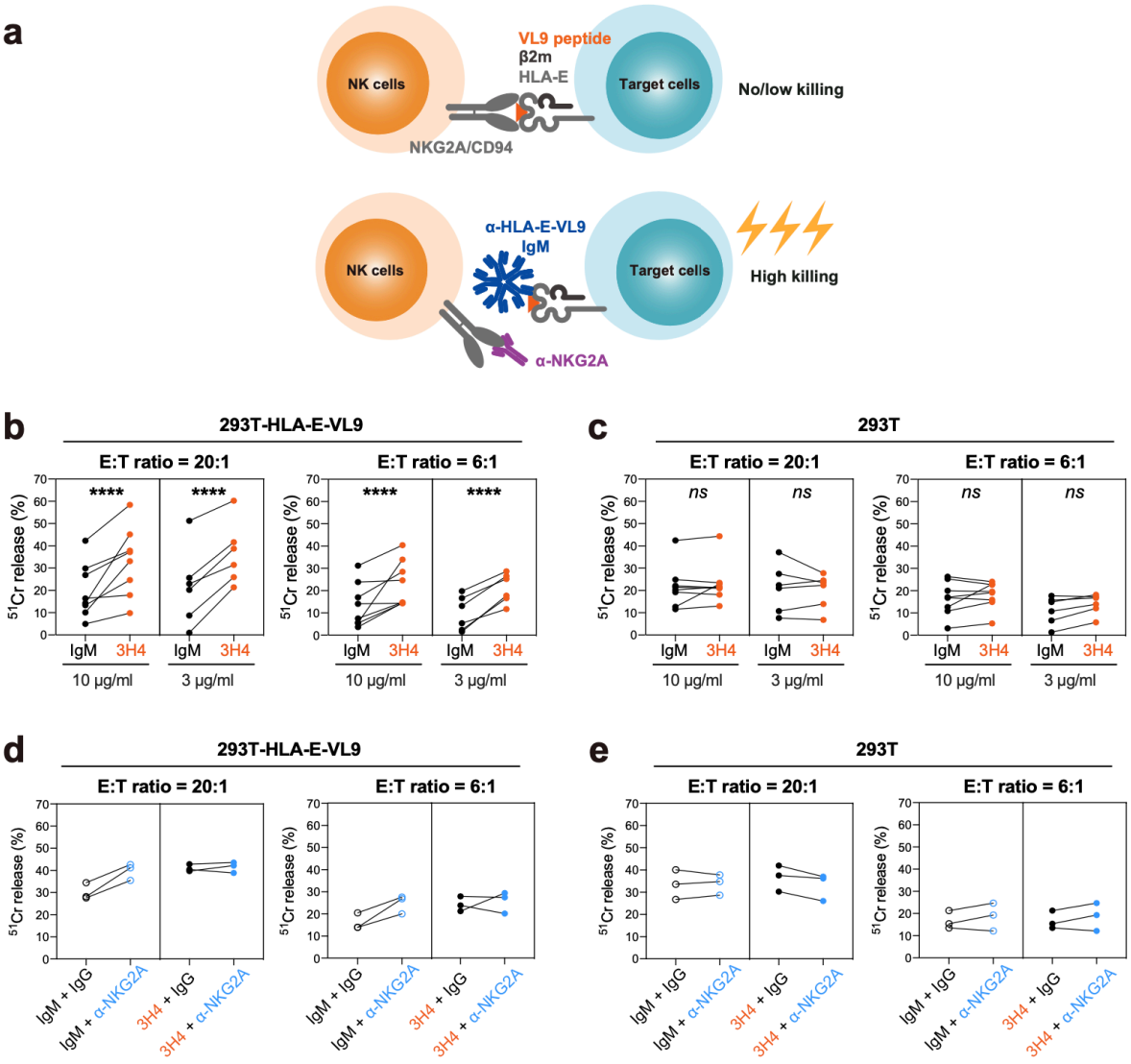

619

620 **Figure. 3 MAb 3H4 enhanced the cytotoxicity of the NKG2A+ NK cell line NK-92 against**

621 **HLA-E-VL9 expressing 293T cells.**

622 **a, Schematic illustrating the hypothesis.** Blockade of the inhibitory NKG2A/CD94/HLA-E

623 pathway with anti-HLA-E-VL9 antibody (3H4) and/or anti-NKG2A antibody (Z199) could

624 enhance target cell lysis by NK cells.

625 **b-c, NK cell cytotoxicity against 3H4 IgM-treated target cells as assessed by ^{51}Cr release**

626 **assay.** Antibody was incubated with HLA-E-VL9 transfected 293T cells (b) and untransfected

627 293T cells (c) at final concentration of 10 μg/ml or 3 μg/ml, and NK92 cells were added into the

628 mixture as effector cells at effector: target (E:T) ratios of 20:1 and 6:1. Mouse IgM MM-30 was
629 used as an isotype controls. Dots represent the mean values of triplicate wells in eight
630 independent experiments. Statistical analysis was performed using mixed effects models.
631 Asterisks show the statistical significance between indicated groups: ns, not significant,
632 *P<0.05, **P<0.01, ***P<0.001, ****P<0.0001.
633 **d-e, NK cell cytotoxicity in the presence of anti-NKG2A mouse IgG Z199 in combination**
634 **with TE4 control- or 3H4- treated target cells as assessed by ^{51}Cr release assay.** Antibody
635 combinations of Z199 + IgM control (d) or Z199 + 3H4 (e) were incubated with HLA-E-VL9
636 transfected 293T cells and untransfected 293T cells at a final concentration of 10 μg/ml, and
637 NK92 cells were added into the mixture as effector cells. Dots represent the mean values of
638 triplicate wells in three independent experiments.
639

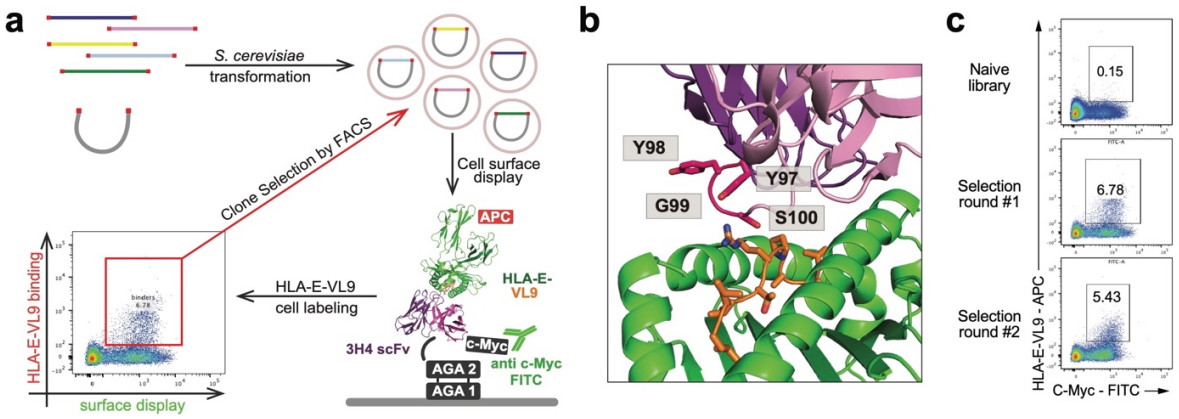

d

3H4 GWT	Y97	Y98	G99	S100
3H4 Gv2	T	A	R	Y
3H4 Gv3	S	A	Q	Y
3H4 Gv4	T	G	R	F
3H4 Gv5	G	A	Q	T
3H4 Gv6	G	A	Q	W
3H4 Gv7	G	A	R	W
3H4 Gv8	A	A	Q	H
3H4 Gv9	A	A	R	F
3H4 Gv10	G	A	R	H
3H4 Gv11	A	A	T	Y
3H4 Gv12	R	G	P	P

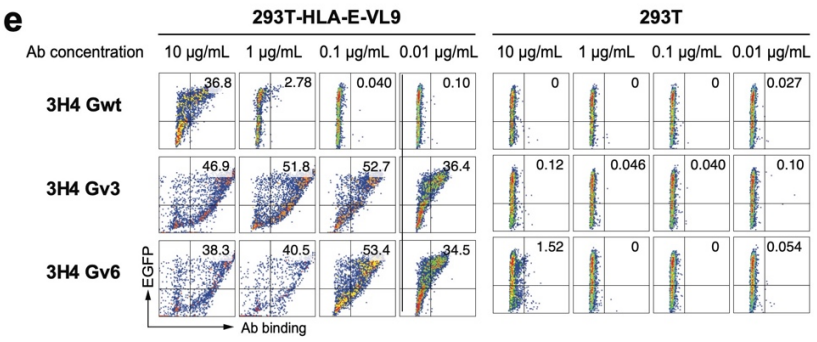

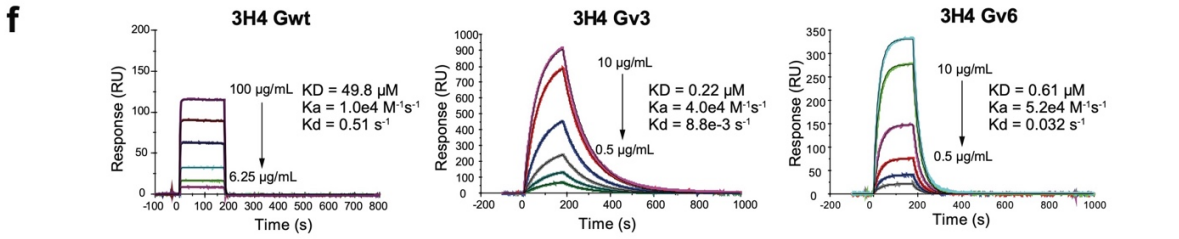

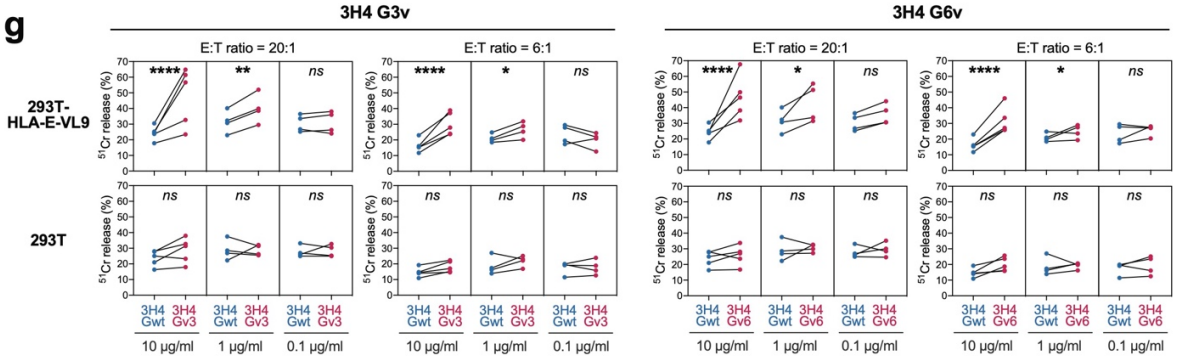

640

641 **Figure. 4 Affinity maturation of HLA-E-VL9-specific antibody 3H4 on human IgG1**
642 **backbone.**
643 **a, Schematic illustration of the affinity maturation strategy.** Libraries of 3H4 mAb variants
644 were transformed into *S. cerevisiae* and displayed on the surface of yeast cells as single-chain
645 fragment variable (scFv). APC-conjugated HLA-E-VL9 tetramers were used for FACS sorting.
646 **b, Sites at the 3H4/HLA-E-VL9 interface where sequence optimization by library**
647 **screening provideed the most significant affinity gains.** 3H4: *purple*; HLA-E: *green*; VL9
648 peptide: *orange*.
649 **c, Enrichement of HLA-E-VL9+ library clones after three rounds of selection by**
650 **fluorescence-activated cell sorting (FACS).** The yeast cells containing the scFv libraries were
651 sorted sequentially for binding to decreasing concentrations of fluorescently labeled HLA-E-VL-9
652 (50 μg/ml, *top*; 10 μg/ml, *middle*; or 0.6 μg/ml *bottom*).
653 **d, Mutations at positions 97-100 in the eleven 3H4 variants chosen for additional**
654 **characterization upon library screening.**
655 **e, Binding of 3H4 Gwt and optimized variants to HLA-E-VL9 or HLA-E-Mtb44 transfected**
656 **293T cells.** Representative flow cytometry data from one of three independent experiments are
657 shown.
658 **f, SPR sensorgrams showing binding kinetics of 3H4 Gwt and optimized variants.** Rate
659 constants (k_a, k_d) and dissociation constant K_D were determined by curve fitting analysis of SPR
660 data with a 1:1 binding model. Binding data are shown as colored lines, and the best fits of a 1:1
661 binding model are shown as black lines. Representative data from one of two independent
662 experiments are shown.
663 **g, Enhanced NK-92 cell cytotoxicity by optimized IgG 3H4 Gv3 and 3H4 Gv6 on HLA-E-**
664 **VL9 transfected 293T cells and untransfected 293T cells, in compare with IgG 3H4 Gwt.**
665 Dots represent the mean values of triplicate wells in four or five independent ^{51}Cr release
666 assays.

667 Statistical analysis was performed using mixed effects models. Asterisks show the statistical
668 significance between indicated groups: ns, not significant, *P<0.05, **P<0.01, ***P<0.001,
669 ****P<0.0001.
670

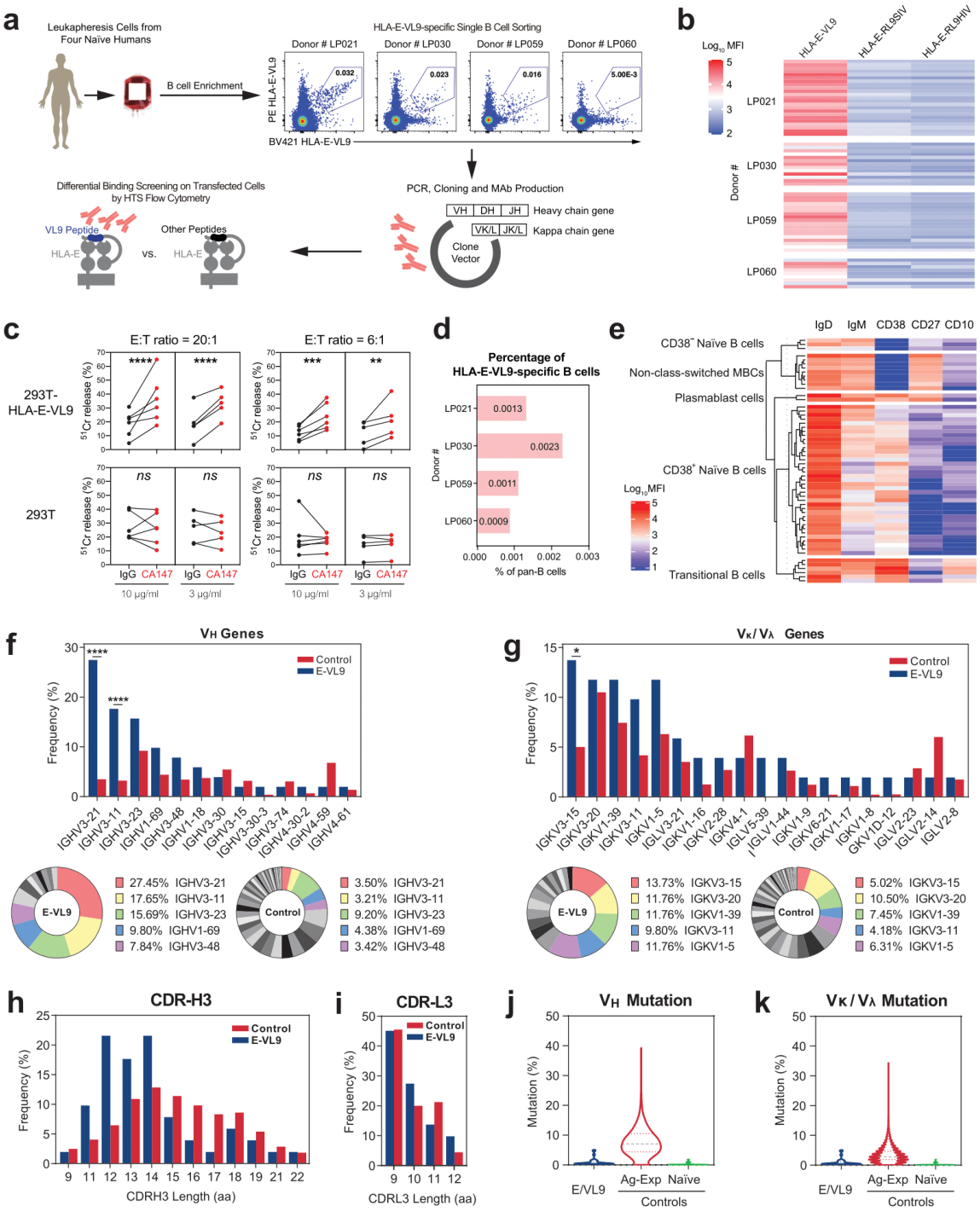

671

672 **Figure. 5 HLA-E-VL9-specific antibodies isolated from the B cell pool of healthy humans.**

673 **a, Scheme of isolating HLA-E-VL9-specific antibodies from healthy humans.** Pan-B cells

674 were first isolated by negative selection from human leukapheresis PBMCs. A three-color

675 sorting strategy was used to sort single B cells that were positive for HLA-E-VL9 and negative
676 for HLA-E-RL9HIV or HLA-E-RL9SIV. Flow cytometry data showing the sorting of HLA-E-VL9
677 double positive, HLA-E-RL9HIV negative, HLA-E-RL9SIV negative B cells in PBMCs from four
678 donors (LP021, LP030, LP059 and LP060) are shown. Variable regions of antibody heavy and
679 light chain genes were isolated from the sorted B cells by PCR, and cloned into an expression
680 backbone with a human IgG1 constant region. Antibodies were produced by transient
681 transfection in 293i cells, and antibody binding specificities were analyzed by surface staining of
682 transfected 293T cells and high throughput screening (HTS) flow cytometry.
683 **b, Binding specificities of the HLA-E-VL9-specific antibodies (*n*=56) from four donors**
684 **shown as a heatmap.** The compensated MFIs of HLA-E-VL9-specific antibody staining on
685 HLA-E-VL9, HLA-E-RL9HIV, or HLA-E-RL9SIV transfected 293T cells at a concentration of 1
686 μg/ml were shown. Representative data from one of two independent experiments are shown.
687 **c, NK cell cytotoxicity against CA147 IgG-treated target cells as assessed by ^{51}Cr release**
688 **assay.** Human antibody CA147 was incubated with HLA-E-VL9 transfected 293T cells and
689 untransfected 293T cells at final concentration of 10 μg/ml or 3 μg/ml, and NK92 cells were
690 added into the mixture as effector cells at effector: target (E:T) ratio of 20:1 and 6:1. Human
691 antibody A32 was used as the isotype control. Dots represent the mean values of triplicate wells
692 in five independent experiments. Statistical analysis was performed using mixed effects models.
693 Asterisks show the statistical significance between indicated groups: ns, not significant,
694 *P<0.05, **P<0.01, ***P<0.001, ****P<0.0001.
695 **d, Percentage of HLA-E-VL9-specific B cells in CD19^{+} pan-B cells in four donors.**
696 **e, Phenotypes of HLA-E-VL9-specific B cells (*n*=56) shown as heatmap.** Expression of
697 markers in each single B cell were determined from index sorting data and are shown as MFIs
698 after compensation. Compensated MFIs below zero were set as zero. Each row indicates one
699 single cell. The rows were clustered by K-means Clustering in R. Four subsets were observed:
700 CD10^{-}CD27^{-}CD38$^{+/-}$ naïve B cells, CD10^{+}CD27^{-}CD38^{++} transitional B cells, CD10^{-}CD27^{+}CD38^{-}

701 non-class-switched memory B cells, and $CD10^{-}CD27^{+}CD38^{+}$ plasmablast cells. Detailed
702 information for each single cell and antibody is shown in ***Table S4***.
703 **f-g, Antibody gene usages. f,** Heavy chain viable (V_H) region gene usage shown as a bar chart
704 (left) and pie chart (right). The top five V_H genes found in HLA-E-VL9-specific antibodies are
705 colored in the pie charts. **g,** Kappa chain variable (V_κ) and lambda chain variable (V_λ) region
706 gene usage shown as a bar chart (left) and pie chart (right). The top five V_κ/V_λ genes found in
707 HLA-E-VL9-specific antibodies are colored in the pie charts. Reference VH-VL repertoires
708 (n=198,148) from three healthy human donors from a previous study (*DeKosky, Nat Med 2015*)
709 were used as a control. The chi-square test of independence was performed to test for an
710 association between indicated gene usage and repertoire/antibody type in panels A-B. ****,
711 $p<0.0001$; *, $0.01<p<0.05$.
712 **h-i, Comparison of heavy chain (h) and light chain (i) CDR3 (CDR-H3) length.** HLA-E-VL9
713 antibody CDR-H3 length was compared with the reference (DeKosky et al., 2015) human
714 antibody CDR-H3 length.
715 **j-k, Violin plots showing the mutation rates of heavy chains (j) and light chains (k).** HLA-
716 E-VL9 antibody sequences (E-VL9) were compared with reference sequences from naïve and
717 antigen-experienced (Ag-Exp) antibody repertoires (n=13,780 and 34,692, respectively).
718
719

Supplementary Materials for

Murine and Human Antibodies that Bind HLA-E-Leader Peptide Complexes and Enhance NK Cell Cytotoxicity

Dapeng Li[1,5,8,9,*], Simon Brackenridge[2,8], Lucy C. Walters[2,8], Olivia Swanson[1], Karl Harlos[3], Daniel Rozbesky[3,4], Derek W. Cain[1,5], Kevin Wiehe[1,5], Richard M. Scearce[1], Maggie Barr[1], Zekun Mu[1], Robert Parks[1], Max Quastel[2], Robert J. Edwards[1,5], Yunfei Wang[1,5], Wes Rountree[1,5], Kevin O. Saunders[1,6,7], Guido Ferrari[7], Persephone Borrow[2], E. Yvonne Jones[3], S. Munir Alam[1,5], Mihai L. Azoitei[1,5,*], Geraldine M. Gillespie[2,*], Andrew J. McMichael[2,*], Barton F. Haynes[1,6,*]

[1]Duke Human Vaccine Institute, Duke University School of Medicine, Durham, NC 27710, USA

[2]Nuffield Department of Clinical Medicine, University of Oxford, Oxford, OX3 7FZ, UK

[3]Division of Structural Biology, Wellcome Centre for Human Genetics, University of Oxford, Oxford, OX3 7BN, UK

[4]Department of Cell Biology, Charles University, Prague, 12800, Czech Republic

[5]Department of Medicine, Duke University School of Medicine, Durham, NC 27710, USA

[6]Department of Immunology, Duke University School of Medicine, Durham, NC 27710, USA

[7]Department of Surgery, Duke University School of Medicine, Durham, NC 27710, USA

[8]Authors contributed equally

[9]Lead contact

*Address correspondence to dapeng.li@duke.edu, mihai.azoitei@duke.edu, geraldine.gillespie@ndm.ox.ac.uk, andrew.mcmichael@ndm.ox.ac.uk and barton.haynes@duke.edu

This PDF file includes:

Materials and Methods

References

Supplementary Figure. S1 to S4

Other Supplementary Material for this manuscript includes the following:

Supplementary Table S1-S4

MATERIALS AND METHODS

Cell Lines

K562-E cells (K562 cells stably expressing HLA-E) and K562-E/UL49.5 cells (with a TAP-inhibitor UL49.5) are kindly provided by Dr. Thorbald van Hall from Leiden University (Lampen et al., 2013). All the other cells used in this study are from ATCC. 293T cells (ATCC CRL-3216) were maintained in Dulbecco's Modified Eagle's Medium (DMEM; Gibco, Catalog# 10564) supplemented with 10% fetal bovine serum (FBS; Gibco, Catalog# 10099141) and 1% penicillin/streptomycin (Gibco, Catalog# 10378016). K562 cells (ATCC CCL-243), K562-E cells and K562-E/UL49.5 cells were cultured in Iscove's Modified Dulbecco's Medium (IMDM; Hyclone, Catalog# SH30228.01) supplemented with 10% FBS. Jurkat, DU-4475 and U-937 cells were cultured in RPMI-1640 medium (Gibco, Catalog# 72400) supplemented with 10% FBS. SiHa cells were cultured in Minimum Essential Medium (MEM; Gibco, Catalog# 11095080) supplemented with 10% FBS. The NK-92 human cell line (ATCC CRL-2407) was cultured in Alpha Minimum Essential medium (α-MEM; Gibco, Catalog# 12561072) supplemented with 2 mM L-glutamine, 0.2 mM inositol, 0.1 mM 2-mercaptoethanol, 0.02 mM folic acid, 100 U/ml recombinant IL-2 (Biolegend, Catalog# 589108), 12.5% horse serum (Gibco, Catalog# 16050122) and 12.5% FBS. All the cells were maintained at 37°C, 5% CO2 in humidified incubators.

Animals

57 Transgenic mice carrying human β2-microglobulin (β2m) and HLA-B*27:05 genes were
58 obtained from Jackson lab (B6.Cg-Tg(B2M,HLA-B*27:05)56-3Trg/DcrJ; stock# 003428).
59 Hemizygous mice were used in this experiment, as this strain is homozygous lethal. For
60 hemizygous mice genotyping, peripheral blood lymphocytes (PBLs) were isolated and
61 stained using mouse CD45 antibody (Biolegend, Catalog# 103122), human HLA class I
62 antibody (Biolegend, Catalog# 311406) and human β2m antibody (Biolegend, Catalog#
63 316312). All animal experiments were conducted with approved protocols from the Duke
64 University Institutional Animal Care and Use Committee.
65
66 **Human Subjects**
67 Human leukapheresis frozen vials were collected by the External Quality Assurance
68 Program Oversight Laboratory (EQAPOL) (Sanchez et al., 2014a; Sanchez et al., 2014b).
69 Samples from four male donors were used in this study. ***Table S5*** shows the clinical
70 characteristics of the individuals studied. All experiments that related to human subjects was
71 carried out with the informed consent of trial participants and in compliance with Institutional
72 Review Board protocols approved by Duke University Medical Center.
73
74 **Peptide synthesis**
75 The VL9 peptide (VMAPRTVLL) was synthesized to >85% purity via Fmoc (9-
76 fluorenylmethoxy carbonyl) chemistry by Genscript USA and reconstituted to 200mM in
77 DMSO.
78
79 **HLA-E-peptide protein refolding and purification**
80 β2-microglobulin, previously purified from inclusion bodies in a Urea-MES buffer, was
81 added to a refolding buffer to achieve a final concentration of 2 μM. The refold buffer
82 comprised 100 mM Tris pH8.0, 400 mM L-arginine monohydrochloride, 2 mM EDTA, 5 mM
83 reduced glutathione and 0.5 mM oxidized Glutathione and was prepared in MiliQ water. A 20
84 μM concentration of VL9 peptide (VMAPRTVLL), previously reconstituted to 200 mM in

85 DMSO, was added to the refolding buffer followed by HLA-E*0103 heavy chain, which was
86 pulsed into the refold to a final concentration of 1 μM. Once the refold had incubated for 72
87 hours at 4 °C it was filtered through a 1.0 μm cellular nitrate membrane and concentrated in
88 the VivaFlow 50R and VivaSpin Turbo Ultrafiltration centrifugal systems with 10 kDa
89 molecular weight cut-offs. The concentrated samples were injected onto a Superdex S75
90 16/60 column and refolded protein eluted according to size into phosphate buffered saline
91 (PBS). Eluted protein complexes were validated by non-reducing SDS-PAGE
92 electrophoresis on NuPAGE 12% Bis-Tris protein gels and further concentrated via VivaSpin
93 Turbo Ultrafiltration centrifugal device to 1.1 mg/mL.
94
95 **HLA-E-peptide biotinylation and tetramer generation**
96 HLA-E-peptide samples requiring biotinylation were subsequently buffered exchanged
97 on Sephadex G-25 PD10 columns (GE Healthcare, UK) into 10mM Tris buffer using
98 commercially available BirA enzyme (Avidity, USA) following the manufacturer's
99 instructions. Following overnight biotinylation, protein samples were subsequently
100 purified into 20mM Tris pH8,100mM NaCl buffer or PBS on a HiLoad 16/600 Superdex 75pg
101 column using an AKTA size exclusion fast protein liquid chromatography (FPLC) system.
102 Correctly folded β2m-HLA-E*01:03-peptide complexes were subsequently concentrated to 2
103 mg/mL and snap frozen.
104 HLA-E*01:03 tetramers were generated via conjugation to various fluorescent labels
105 including Extravidin-PE (Sigma), Streptavidin-bound APC (Biolegend, San Diego) or BV421
106 (Biolegend, San Diego) at a Molar ratio of 4:1 as previously described (Braud et al., 1998).
107
108 **Immunization in HLA-B27/β2m Transgenic Mice**
109 HLA-B27/β2m transgenic mice (*n*=23) were intramuscularly (i.m.) immunized with
110 pooled HLA-E-RL9HIV complex (12.5 μg/animal) and HLA-E-RL9SIV complex (12.5
111 μg/animal) adjuvanted with STR8S-C (Moody et al., 2014) at weeks 0, 2, 4, 6, 12 and 16.
112 MAb 3H4 was isolated from this study. In another experiment, HLA-B27/β2m transgenic

113 mice (*n* = 10) were i.p. immunized with either HLA-E-RL9HIV single chain trimer (SCT)
114 transfected 293T cells (2x10^6 cells/animal) or HLA-E-RL9SIV SCT transfected 293T cells
115 (2x10^6 cells/animal) at weeks 0, 2, 4, 6, 17 and 19. MAb 13F11 was isolated from this study.
116 In the third experiment, HLA-B27/β2m transgenic mice (*n*=10) were i.m. immunized with
117 HLA-E-VL9 complex (25 μg/animal) adjuvanted with STR8S-C at Week 0, 2 and 4, following
118 by intraperitoneally (i.p.) immunization with HLA-E-VL9 SCT transfected 293T cells (2x10^6
119 cells/animal) at Week 14, 16 and 18. MAb 10C10 and 2D6 were isolated from this study.
120 Serum titers were monitored by ELISA Mice with high binding antibody titers were selected
121 for the subsequent spleen cell fusion and B cell sorting experiments.
122
123 **Hybridoma Cell Line Generation and Monoclonal Antibody Production**
124 Mice were boosted with the indicated priming antigen 3 days prior to fusion. Spleen cells
125 were harvested and fused with NS0 murine myeloma cells using PEG1500 to generate
126 hybridomas. After 2 weeks, supernatant of hybridoma clones were collected and screened
127 by flow cytometry-based high throughput screening (HTS). Specifically, we tested for
128 antibodies differentially binding 293T cells transiently transfected with plasmid DNA
129 expressing single chain peptide-HLA-E-ß2m trimers so that they expressed HLA-E-RL9HIV,
130 HLA-E-RL9SIV or HLA-E-VL9 at the cell surface. Hybridomas cells that secreted HLA-E-VL9
131 antibodies were cloned by limiting dilution for at least 5 rounds until the phenotypes of all
132 limiting dilution wells are identical. IgG mAbs were purified by protein G affinity
133 chromatography, while IgM mAbs were purified by ammonium sulfate precipitation and by
134 Superose 6 column size-exclusion chromatography in AKTA Fast Protein Liquid
135 Chromatography (FPLC) system. The VH and VL sequences of mAbs were amplified from
136 hybridoma cell RNA using primers reported previously (Tian et al., 2016; von Boehmer et al.,
137 2016).
138
139 **Cell Surface Staining and High-Throughput Screening (HTS)**

140 HLA-E SCT constructs encoding HLA-E-VL9, HLA-E-RL9HIV, or HLA-E-RL9SIV were
141 transfected into 293T cells using GeneJuice transfection reagent (Novagen, Catalog#
142 70967). For epitope mapping experiment, a panel of HLA-E-VL9 SCT constructs with single
143 amino acid mutations were transfected into 293T cells using the same method. Cells were
144 dissociated with 0.1% EDTA at 48 hours post-transfection and stained with a Fixable Near-
145 IR Dead Cell Stain Kit (Thermo Fisher, Catalog# L34976). After washing, primary antibodies
146 (supernatant from hybridoma cells, supernatant from transfected cells, or purified antibodies)
147 were added and incubated with cells for 1 hour at 4°C, following by staining with 1:1000
148 diluted secondary antibodies for 30 mins at 4°C. For mouse primary antibodies, we used
149 Alexa Fluor 555 (AF555) conjugated goat anti-mouse IgG (H+L) (Thermo Fisher, Catalog#
150 A32727) or Alexa Fluor 647 (AF647) conjugated goat anti-mouse IgG (H+L) (Thermo Fisher,
151 Catalog# A32728) as secondary antibodies; for human primary antibodies, we used AF555
152 conjugated goat anti-human IgG (H+L) (Thermo Fisher, Catalog# A-21433) or AF647
153 conjugated goat anti-human IgG (H+L) (Thermo Fisher, Catalog# A-21445) as secondary
154 antibodies. Cells were then washed 3 times and resuspended in fixation buffer (1%
155 formaldehyde in PBS, pH7.4). Data were acquired on a BD LSR II flow cytometer and
156 analyzed using FlowJo version 10.
157
158 **3H4 Fab production**
159 A humanized version of the 3H4 antibody (3H4-huIgG1) was digested to produce Fab
160 fragments using the Pierce Fab Preparation kit (ThermoFisher SCIENTIFIC). 3H4 Fab-
161 retrieved sample was further purified by size exclusion on a Superdex S75 16/60 column
162 and eluted into PBS buffer. Following concentration to 1.1mg/mL and SDS-PAGE gel-based
163 validation, 3H4 Fab purified material was incubated for 1 hours on ice with freshly purified
164 HLA-E-VL9. The combined 3H4:Fab-HLA-E-VL9 sample was concentrated to 7.5mg/mL
165 prior to crystallographic set-up.
166
167 **Crystallization screening**

168 Crystals were grown via sitting drop vapour-diffusion at 20 °C in a 200nL drop with a 1:1
169 protein to reservoir ratio (Walter et al., 2005). The 3H4 Fab-HLA-E(VL9) co-complex
170 crystallized in 20% PEG 8000, 0.1 M Na HEPES at pH 7, in the ProPlex sparse matrix
171 screen. Crystals were cryo-preserved in 25% glycerol and diffraction data were collected at
172 the I03 beamline of Diamond Light Source.
173
174 **Crystallographic analysis**
175 Two copies of the co-complex structure of 3H4 Fab bound to HLA-E-VL9 were present
176 in the asymmetric unit, a single copy constituted the focus of further discussion since root-
177 mean-square deviation (RMSD) calculations from Cα-atom pairwise alignment of the two
178 copies indicated minimal repositioning of interfacing residues at the HLA-E-3H4 binding site
179 (***Table S2B-F***). Additionally, pairwise alignment with the previously published non-receptor-
180 bound HLA-E coordinates (PDB ID: 1MHE) (O'Callaghan et al., 1998) revealed minimal
181 structural changes in HLA-E upon 3H4 engagement (***Table S2C***).
182 Diffraction data were merged and indexed in xia2 dials (Winter et al., 2018). Outer shell
183 reflections were excluded from further analysis to ensure the $CC_{1/2}$ value exceeded the
184 minimum threshold (>0.5) in each shell (Karplus and Diederichs, 2012). Sequential
185 molecular replacement was carried out in MolRep of the CCP4i suite using molecule one of
186 the previously published Mtb44-bound HLA-E structure with the peptide coordinates deleted
187 (PDB ID: 6GH4) and one molecule of the previously published anti-APP-tag Fab structure
188 (PDB ID: 6HGU) as phasing models (Vagin and Teplyakov, 2010; Winn et al., 2011). Rigid
189 body and retrained refinement were subsequently carried out by Phenix.refine (Afonine et
190 al., 2012) in between manual model building in Coot (Emsley et al., 2010). Model geometry
191 was validated by MolProbity (Chen et al., 2010) and structural interpretation was conducted
192 using the PyMOL Molecular Graphics System, version 2.0 (Schrödinger, LLC) in addition to
193 the PDBePISA (Krissinel and Henrick, 2007) and PDBeFOLD (Krissinel and Henrick, 2004)
194 servers.
195

196 **Antigen-Specific Single B Cell Sorting**

197 HLA-E-VL9-specific human B cells were sorted in flow cytometry using a three-color
198 sorting technique. Briefly, the stabilized HLA-E-β2M-peptide complexes were made as
199 tetramers and conjugated with different fluorophores. Human pan-B cells, including naïve
200 and memory B cells, were isolated from PBMCs of healthy donors using human pan-B cell
201 enrichment kit (STEMCELL, Catalog# 19554). The isolated pan-B cells were then stained
202 with IgM PerCp-Cy5.5 (Clone# G20-127, BD Biosciences, Catalog# 561285), IgD FITC
203 (Clone# IA6-2, BD Biosciences, Catalog# 555778), CD3 PE-Cy5 (Clone# HIT3a, BD
204 Biosciences, Catalog# 555341), CD235a PE-Cy5 (Clone# GA-R2, BD Biosciences,
205 Catalog# 559944), CD10 PE-CF594 (Clone# HI10A, BD Biosciences, Catalog# 562396),
206 CD27 PE-Cy7 (Clone# O323, eBioscience, Catalog# 25-0279), CD16 BV570 (Clone# 3G8,
207 Biolegend, Catalog# 302035), CD14 BV605 (Clone# M5E2, Biolegend, Catalog# 301834),
208 CD38 APC-AF700 (Clone# LS198-4-2, Beckman Coulter, Catalog# B23489), CD19 APC-
209 Cy7 (Clone# LJ25C1, BD Biosciences, Catalog# 561743) and tetramers at 2 μg/million cells
210 (including BV421-conjugated HLA-E-VL9 tetramer, PE-conjugated HLA-E-VL9 tetramer,
211 APC-conjugated HLA-E-RL9SIV tetramer and APC-conjugated HLA-E-RL9HIV tetramer).
212 The cells were then stained with a Fixable Aqua Dead Cell Stain Kit (Invitrogen, Catalog#
213 L34957). HLA-E-VL9-specific B cells were sorted in BD FACSAria II flow cytometer (BD
214 Biosciences) for viable $CD3^{neg}$/ $CD14^{neg}$ /$CD16^{neg}$ /$CD235a^{neg}$/$CD19^{pos}$ / HLA-E-$VL9^{double\text{-}pos}$/
215 HLA-E-$RL9HIV^{neg}$/HLA-E-$RL9SIV^{neg}$ subset as single cells in 96-well plates.

216

217 **PCR Amplification of Human Antibody Genes**

218 The $V_HD_HJ_H$ and V_LJ_L genes were amplified by RT-PCR from the flow cytometry-sorted
219 single B cells using the methods as described previously (Liao et al., 2009; Wrammert et al.,
220 2008) with modification. Primer details were listed in Tables S2. The PCR-amplified genes
221 were then purified and sequenced with 10 μM forward and reverse primers. Sequences were
222 analyzed by using the human library in Clonalyst for the VDJ arrangements of the
223 immunoglobulin *IGHV*, *IGKV*, and *IGLV* sequences and mutation frequencies (Kepler et al.,

224 2014). Clonal relatedness of $V_HD_HJ_H$ and V_LJ_L sequences was determined as previously
225 described (Liao et al., 2013).
226
227 **Expression of $V_HD_HJ_H$ and V_LJ_L as Full-Length IgG Recombinant mAbs**
228 Transient transfection of recombinant mAbs was performed as previously described
229 (Liao et al., 2009). Briefly, purified PCR products were used for overlapping PCR to generate
230 linear human antibody expression cassettes. The expression cassettes were transfected into
231 293i cells using ExpiFectamine (Thermo Fisher Scientific, Catalog# A14525). The
232 supernatant samples containing recombinant antibodies were used for cell surface staining
233 and HTS assay to measure the binding reactivities.
234 The selected human antibody genes were then synthesized and cloned (GenScript) in a
235 human IgG1 backbone with 4A mutations (Saunders, 2019). Recombinant IgG mAbs were
236 then produced in HEK293i suspension cells by transfection with ExpiFectamine and purified
237 using Protein A resin. The purified mAbs were run in SDS-PAGE for Coomassie blue
238 staining and western blot. Antibodies with aggregation were further purified in AKTA FPLC
239 system using a Superdex 200 size-exclusion column.
240
241 **Surface Plasmon Resonance (SPR)**
242 Surface plasmon resonance assays were performed on a BIAcore 3000 instrument, and
243 data analysis was performed with BIAevaluation 3.0 software as previously described (Liao
244 et al., 2006). Purified mAbs flowed over CM5 sensor chips at concentrations of 100 µg/ml,
245 and antibody binding was monitored in real-time at 25°C with a continuous flow of PBS at 30
246 µl/min. For SPR affinity measurements, antibody binding to HLA-E-VL9 complex protein was
247 performed using a BIAcore S200 instrument (Cytiva, formerly GE Healthcare, DHVI BIA
248 Core Facility, Durham, NC) in HBS-EP+ 1x running buffer. The antibodies were first
249 captured onto CM5 sensor chip to a level of ~9000 RU. The HLA-E-VL9 soluble proteins
250 were injected over the captured antibodies at a flow rate of 30uL/min. After dissociation, the
251 antibodies were regenerated using a 30 second pulse of Glycine pH2.0. Results were

252 analyzed using the Biacore S200 Evaluation software (Cytiva). Subsequent curve fitting
253 analyses were performed using a 1:1 Langmuir model with a local Rmax. The reported
254 binding curves are representative of two data sets.
255
256 **ELISA**
257 Direct binding ELISAs were conducted in 384-well ELISA plates coated with 2 µg/ml of
258 C-trap-stabilized HLA-E-VL9, C-trap-stabilized HLA-E-RL9HIV or C-trap-stabilized HLA-E-
259 RL9SIV in 0.1 M sodium bicarbonate overnight at 4°C. Plates were washed with PBS +
260 0.05% Tween 20 and blocked with 3% BSA in PBS at room temperature for 1 h. MAb
261 samples were incubated for 1 h in 3-fold serial dilutions starting at 100 µg/ml, followed by
262 washing with PBS-0.05% Tween 20. HRP-conjugated goat anti-human IgG secondary Ab
263 (SouthernBiotech, catalog# 2040-05) was diluted to 1: 10,000 in 1% BSA in PBS-0.05%
264 Tween 20 and incubated at room temperature for 1 h. For sandwich ELISA, 384-well ELISA
265 plates were coated with HLA-E-VL9 antibodies in a 3-fold dilution starting from 100 µg/mL in
266 0.1 M sodium bicarbonate overnight at 4°C. Plates were washed with PBS + 0.05% Tween
267 20 and blocked with 3% BSA in PBS at room temperature for 1 h. C-trap-stabilized HLA-E-
268 VL9, C-trap-stabilized HLA-E-RL9HIV, C-trap-stabilized HLA-E-RL9SIV, or diluent control
269 were then added at 2 µg/mL and incubated at room temperature for 1 h. After washing,
270 HRP-conjugated anti-human β2M antibody (Biolegend, catalog# 280303) were added at 0.2
271 µg/mL and incubated at room temperature for 1 h. These plates were washed for 4 times
272 and developed with tetramethylbenzidine substrate (SureBlue Reserve). The reaction was
273 stopped with 1 M HCl, and optical density at 450 nm (OD_{450}) was determined.
274
275 **Antibody Poly-Reactivity Assays**
276 All mAbs isolated from mice and human were tested for ELISA binding to nine
277 autoantigens - Sjogren's syndrome antigen A (SSA), Sjogren's syndrome antigen (SSB),
278 Smith antigen (Sm), ribonucleoprotein (RNP), scleroderma 70 (Scl-70), Jo-1 antigen,
279 double-stranded DNA (dsDNA), centromere B (Cent B), and histone as previously described

280 (Han et al., 2017; Liao et al., 2011). Indirect immunofluorescence assay of mAbs binding to
281 HEp-2 cells (Inverness Medical Professional Diagnostics, Princeton, NJ) was performed as
282 previously described (Haynes et al., 2005; Liao et al., 2011). MAbs 2F5 (Yang et al., 2013)
283 and 17B (Moore and Sodroski, 1996) were used as positive and negative controls,
284 respectively. All antibodies were screened in two independent experiments.
285
286 **Negative Stain Electron Microscopy of IgM antibodies**
287 FPLC purified IgM antibodies were diluted to 0.08 mg/ml in HEPES-buffered saline (pH
288 7.4) + 5% glycerol, and stained with 2% uranyl formate. Images were obtained with a Philips
289 EM420 electron microscope at 82,000 magnification and processed in Relion 3.0.
290
291 **Peptide-Pulsing in K562-E Cells**
292 K562-E cells and K562-E/UL49.5 cells were resuspended with fresh IMDM media with
293 10% FBS at $2x10^6$ cells/ml. Peptides were added into cell suspension at a final
294 concentration of 100 μM. The cell/peptide mixtures were incubated at 26°C with 5% CO_2 for
295 20-22 hours and were transferred to 37°C for 2 hours with 5% CO_2 before use. In the
296 following mAb staining experiment, medium with 100 μM peptides was used to maintain
297 peptide concentration.
298
299 **NK Cell Cytotoxicity Assay**
300 NK Cell Cytotoxicity was measured by ^{51}Cr release assay. A NKG2A-positive,
301 CD16/CD32/CD64-negative NK-92 cells were used as effector cells in our study.
302 Transfected or untransfected 293T cells were used as target cells. Target cells were
303 counted, washed, resuspended in R10 at 1×10^7 cell/ml, and labeled with $Na_2{}^{51}CrO_4$ at 250
304 μCi/ml for 2 hours at 37°C. After washing three times using R10, cells were mixed with the
305 testing antibody and effector cells in a final effector to target (E:T) ratio of 20:1 and 6:1 in
306 triplicate wells in a flexible 96 well round bottom plates (PerkinElmer, Catalog# 1450-401).
307 The plates were inserted in flexible 96-well plate cassettes (PerkinElmer, Catalog# 1450-

308 101), sealed and incubated at 37°C for 4 hours. After the incubation, cells were pelleted by
309 centrifugation, and from the top of the well, add 25 ul of supernatant to a rigid 96 well
310 isoplates (PerkinElmer, Catalog#1450-514) containing 150 ul of Ultima Gold LSC Cocktail
311 (Sigma, Catalog# L8286). The plates were inserted in rigid 96-well plate cassettes
312 (PerkinElmer, Catalog# 1450-105), sealed and counted on Perkin Elmer Microbeta Triux
313 1450 counter. ^{51}Cr labeled target cells without effector cells were set as a spontaneous
314 release control, and ^{51}Cr labeled target cells mixed with detergent (2% Triton X-100) were
315 used as a maximum release control. The percentages of specific lysis were calculated with
316 the formulation: The Percentages of Specific Lysis (^{51}Cr Release %) = [(Experimental
317 Release – Spontaneous Release)/ (Maximum Release – Spontaneous Release)] x 100.
318
319 **Development and screening of scFv libraries on the surface of yeast**
320 A library was built that contained ~1.1 million 3H4 scFv variants with amino acid
321 diversity at sites that were determined by structural analysis to interact with HLA-E-VL9.
322 Seventeen residues (***Figure. S3***) located in the CDR loops of 3H4 were randomized in
323 groups of four based on their proximity and all the possible combinations of amino acids
324 were sampled at these sites. Library DNA was synthesized on a BioXP 3250 (Codex)
325 system and amplified with High Fidelity Phusion polymerase (New England Biolabs). PCR
326 products were gel extracted (Qiagen Gel Extraction kit) to select full length genes as per the
327 manufacturer's protocol. 3H4 scFv variants were displayed in library format on the surface of
328 yeast as previously described (Benatuil et al., 2010; Chao et al., 2006). Briefly, *S. cerevisiae*
329 EBY100 cells were transformed by electroporation with a 3:1 ratio of 12 µg scFv library DNA
330 and 4 µg pCTcon2 plasmid digested with BamHI, SalI, NheI (New England Biolabs). The
331 size of the transformed library, determined by serial dilution on selective plates, was $5x10^7$
332 individual colonies. Yeast Libraries were grown in SDCAA media (Teknova) supplemented
333 with pen-strep at 30°C and 225 rpm. 80% of the sequences recovered from the transformed
334 libraries were confirmed to contain full length, in-frame genes by Sanger sequencing
335 (Genewiz). scFv expression on the surface of yeast was induced by culturing the libraries in

336 SGCAA (Teknova) media at a density of $1x10^7$ cells/mL for 24-36 hours. Cells were washed
337 twice in ice cold PBSA (0.01M sodium phosphate, pH 7.4, 0.137M sodium chloride, 1g/L
338 bovine serum albumin) and labeled with APC conjugated HLA-E-VL9 tetramer and 1:100
339 anti-c-myc:FITC (ICL) and incubated for 1 hour at 4C. Initial selection was conducted with
340 50mg/mL labeling concentration of HLA-E-VL9 tetramer; the second round of selection was
341 done at 0.6mg/mL tetramer. Cells were washed twice with PBSA after incubation with the
342 fluorescently labeled probes and sorted on a BD FACS-DiVa. Double positive cells for APC
343 and FITC were collected and expanded in SDCAA media supplemented with pen-strep
344 before successive rounds of enrichment. FACS data was analyzed with Flowjo_v10.7
345 software (Becton, Dickinson & Company). All clones selected by FACS were expanded, and
346 their DNA was extracted (Zymo Research) for analysis by Sanger sequencing (Genewiz).
347 scFv encoding plasmids were recovered from yeast cultures by yeast miniprep with the
348 Zymoprep yeast plasmid miniprep II kit (Zymo Research). Isolated DNA was transformed
349 into NEB5α strain of *E. coli* (New England Biolabs) and the DNA of individual bacterial
350 colonies was isolated (Wizard Plus SV Minipreps, Promega) and analyzed by Sanger
351 sequencing (Genewiz).
352
353 **Statistics Analysis**
354 Data were plotted using Prism GraphPad 8.0 or visualized using the ComplexHeatmap
355 R package. SAS 9.4 (SAS Institute, Cary, NC) was used to perform the statistical analysis
356 with a p-value < 0.05 considered significant. For ^{51}Cr release assays, mixed effects models
357 were used to make comparisons of antibody to control using a random intercept for the
358 triplicates run within each experiment and fixed effects of E:T ratio, type (antibody or
359 control), and the interaction of E:T ratio by type. For human antibody gene usage
360 analysis, chi-square test of independence was used to compare differences between
361 groups.
362
363

364 **REFERENCES**

365 Afonine, P.V., Grosse-Kunstleve, R.W., Echols, N., Headd, J.J., Moriarty, N.W., Mustyakimov,
366 M., Terwilliger, T.C., Urzhumtsev, A., Zwart, P.H., and Adams, P.D. (2012). Towards
367 automated crystallographic structure refinement with phenix.refine. Acta Crystallogr D Biol
368 Crystallogr *68*, 352-367.

369 Benatuil, L., Perez, J.M., Belk, J., and Hsieh, C.M. (2010). An improved yeast transformation
370 method for the generation of very large human antibody libraries. Protein Eng Des Sel *23*,
371 155-159.

372 Braud, V.M., Allan, D.S., O'Callaghan, C.A., Soderstrom, K., D'Andrea, A., Ogg, G.S., Lazetic,
373 S., Young, N.T., Bell, J.I., Phillips, J.H.*, et al.* (1998). HLA-E binds to natural killer cell receptors
374 CD94/NKG2A, B and C. Nature *391*, 795-799.

375 Chao, G., Lau, W.L., Hackel, B.J., Sazinsky, S.L., Lippow, S.M., and Wittrup, K.D. (2006).
376 Isolating and engineering human antibodies using yeast surface display. Nature Protocols *1*,
377 755-768.

378 Chen, V.B., Arendall, W.B., 3rd, Headd, J.J., Keedy, D.A., Immormino, R.M., Kapral, G.J.,
379 Murray, L.W., Richardson, J.S., and Richardson, D.C. (2010). MolProbity: all-atom structure
380 validation for macromolecular crystallography. Acta Crystallogr D Biol Crystallogr *66*, 12-21.

381 Emsley, P., Lohkamp, B., Scott, W.G., and Cowtan, K. (2010). Features and development of
382 Coot. Acta Crystallogr D Biol Crystallogr *66*, 486-501.

383 Han, Q., Williams, W.B., Saunders, K.O., Seaton, K.E., Wiehe, K.J., Vandergrift, N., Von Holle,
384 T.A., Trama, A.M., Parks, R.J., Luo, K.*, et al.* (2017). HIV DNA-Adenovirus Multiclade
385 Envelope Vaccine Induces gp41 Antibody Immunodominance in Rhesus Macaques. J Virol
386 *91*.

387 Haynes, B.F., Fleming, J., St Clair, E.W., Katinger, H., Stiegler, G., Kunert, R., Robinson, J.,
388 Scearce, R.M., Plonk, K., Staats, H.F.*, et al.* (2005). Cardiolipin polyspecific autoreactivity in
389 two broadly neutralizing HIV-1 antibodies. Science *308*, 1906-1908.

390 Karplus, P.A., and Diederichs, K. (2012). Linking crystallographic model and data quality.
391 Science *336*, 1030-1033.

392 Kepler, T.B., Munshaw, S., Wiehe, K., Zhang, R., Yu, J.S., Woods, C.W., Denny, T.N.,
393 Tomaras, G.D., Alam, S.M., Moody, M.A.*, et al.* (2014). Reconstructing a B-Cell Clonal
394 Lineage. II. Mutation, Selection, and Affinity Maturation. Front Immunol *5*, 170.
395 Krissinel, E., and Henrick, K. (2004). Secondary-structure matching (SSM), a new tool for fast
396 protein structure alignment in three dimensions. Acta Crystallogr D Biol Crystallogr *60*, 2256-
397 2268.
398 Krissinel, E., and Henrick, K. (2007). Inference of macromolecular assemblies from crystalline
399 state. J Mol Biol *372*, 774-797.
400 Lampen, M.H., Hassan, C., Sluijter, M., Geluk, A., Dijkman, K., Tjon, J.M., de Ru, A.H., van
401 der Burg, S.H., van Veelen, P.A., and van Hall, T. (2013). Alternative peptide repertoire of
402 HLA-E reveals a binding motif that is strikingly similar to HLA-A2. Mol Immunol *53*, 126-131.
403 Liao, H.X., Chen, X., Munshaw, S., Zhang, R., Marshall, D.J., Vandergrift, N., Whitesides, J.F.,
404 Lu, X., Yu, J.S., Hwang, K.K.*, et al.* (2011). Initial antibodies binding to HIV-1 gp41 in acutely
405 infected subjects are polyreactive and highly mutated. J Exp Med *208*, 2237-2249.
406 Liao, H.X., Levesque, M.C., Nagel, A., Dixon, A., Zhang, R., Walter, E., Parks, R., Whitesides,
407 J., Marshall, D.J., Hwang, K.K.*, et al.* (2009). High-throughput isolation of immunoglobulin
408 genes from single human B cells and expression as monoclonal antibodies. J Virol Methods
409 *158*, 171-179.
410 Liao, H.X., Lynch, R., Zhou, T., Gao, F., Alam, S.M., Boyd, S.D., Fire, A.Z., Roskin, K.M.,
411 Schramm, C.A., Zhang, Z.*, et al.* (2013). Co-evolution of a broadly neutralizing HIV-1 antibody
412 and founder virus. Nature *496*, 469-476.
413 Liao, H.X., Sutherland, L.L., Xia, S.M., Brock, M.E., Scearce, R.M., Vanleeuwen, S., Alam,
414 S.M., McAdams, M., Weaver, E.A., Camacho, Z.*, et al.* (2006). A group M consensus envelope
415 glycoprotein induces antibodies that neutralize subsets of subtype B and C HIV-1 primary
416 viruses. Virology *353*, 268-282.
417 Moody, M.A., Santra, S., Vandergrift, N.A., Sutherland, L.L., Gurley, T.C., Drinker, M.S., Allen,
418 A.A., Xia, S.M., Meyerhoff, R.R., Parks, R.*, et al.* (2014). Toll-like receptor 7/8 (TLR7/8) and

419 TLR9 agonists cooperate to enhance HIV-1 envelope antibody responses in rhesus macaques.
420 J Virol *88*, 3329-3339.
421 Moore, J.P., and Sodroski, J. (1996). Antibody cross-competition analysis of the human
422 immunodeficiency virus type 1 gp120 exterior envelope glycoprotein. J Virol *70*, 1863-1872.
423 O'Callaghan, C.A., Tormo, J., Willcox, B.E., Braud, V.M., Jakobsen, B.K., Stuart, D.I.,
424 McMichael, A.J., Bell, J.I., and Jones, E.Y. (1998). Structural features impose tight peptide
425 binding specificity in the nonclassical MHC molecule HLA-E. Mol Cell *1*, 531-541.
426 Sanchez, A.M., DeMarco, C.T., Hora, B., Keinonen, S., Chen, Y., Brinkley, C., Stone, M.,
427 Tobler, L., Keating, S., Schito, M.*, et al.* (2014a). Development of a contemporary globally
428 diverse HIV viral panel by the EQAPOL program. J Immunol Methods *409*, 117-130.
429 Sanchez, A.M., Rountree, W., Berrong, M., Garcia, A., Schuetz, A., Cox, J., Frahm, N., Manak,
430 M., Sarzotti-Kelsoe, M., D'Souza, M.P.*, et al.* (2014b). The External Quality Assurance
431 Oversight Laboratory (EQAPOL) proficiency program for IFN-gamma enzyme-linked
432 immunospot (IFN-gamma ELISpot) assay. J Immunol Methods *409*, 31-43.
433 Saunders, K.O. (2019). Conceptual Approaches to Modulating Antibody Effector Functions
434 and Circulation Half-Life. Front Immunol *10*, 1296.
435 Tian, M., Cheng, C., Chen, X., Duan, H., Cheng, H.L., Dao, M., Sheng, Z., Kimble, M., Wang,
436 L., Lin, S.*, et al.* (2016). Induction of HIV Neutralizing Antibody Lineages in Mice with Diverse
437 Precursor Repertoires. Cell *166*, 1471-1484 e1418.
438 Vagin, A., and Teplyakov, A. (2010). Molecular replacement with MOLREP. Acta Crystallogr
439 D Biol Crystallogr *66*, 22-25.
440 von Boehmer, L., Liu, C., Ackerman, S., Gitlin, A.D., Wang, Q., Gazumyan, A., and
441 Nussenzweig, M.C. (2016). Sequencing and cloning of antigen-specific antibodies from
442 mouse memory B cells. Nat Protoc *11*, 1908-1923.
443 Walter, T.S., Diprose, J.M., Mayo, C.J., Siebold, C., Pickford, M.G., Carter, L., Sutton, G.C.,
444 Berrow, N.S., Brown, J., Berry, I.M.*, et al.* (2005). A procedure for setting up high-throughput
445 nanolitre crystallization experiments. Crystallization workflow for initial screening, automated
446 storage, imaging and optimization. Acta Crystallogr D Biol Crystallogr *61*, 651-657.

447 Winn, M.D., Ballard, C.C., Cowtan, K.D., Dodson, E.J., Emsley, P., Evans, P.R., Keegan, R.M.,
448 Krissinel, E.B., Leslie, A.G., McCoy, A.*, et al.* (2011). Overview of the CCP4 suite and current
449 developments. Acta Crystallogr D Biol Crystallogr *67*, 235-242.
450 Winter, G., Waterman, D.G., Parkhurst, J.M., Brewster, A.S., Gildea, R.J., Gerstel, M.,
451 Fuentes-Montero, L., Vollmar, M., Michels-Clark, T., Young, I.D.*, et al.* (2018). DIALS:
452 implementation and evaluation of a new integration package. Acta Crystallogr D Struct Biol
453 *74*, 85-97.
454 Wrammert, J., Smith, K., Miller, J., Langley, W.A., Kokko, K., Larsen, C., Zheng, N.Y., Mays,
455 I., Garman, L., Helms, C.*, et al.* (2008). Rapid cloning of high-affinity human monoclonal
456 antibodies against influenza virus. Nature *453*, 667-671.
457 Yang, G., Holl, T.M., Liu, Y., Li, Y., Lu, X., Nicely, N.I., Kepler, T.B., Alam, S.M., Liao, H.X.,
458 Cain, D.W.*, et al.* (2013). Identification of autoantigens recognized by the 2F5 and 4E10
459 broadly neutralizing HIV-1 antibodies. J Exp Med *210*, 241-256.
460
461

SUPPLEMENTAL FIGURES

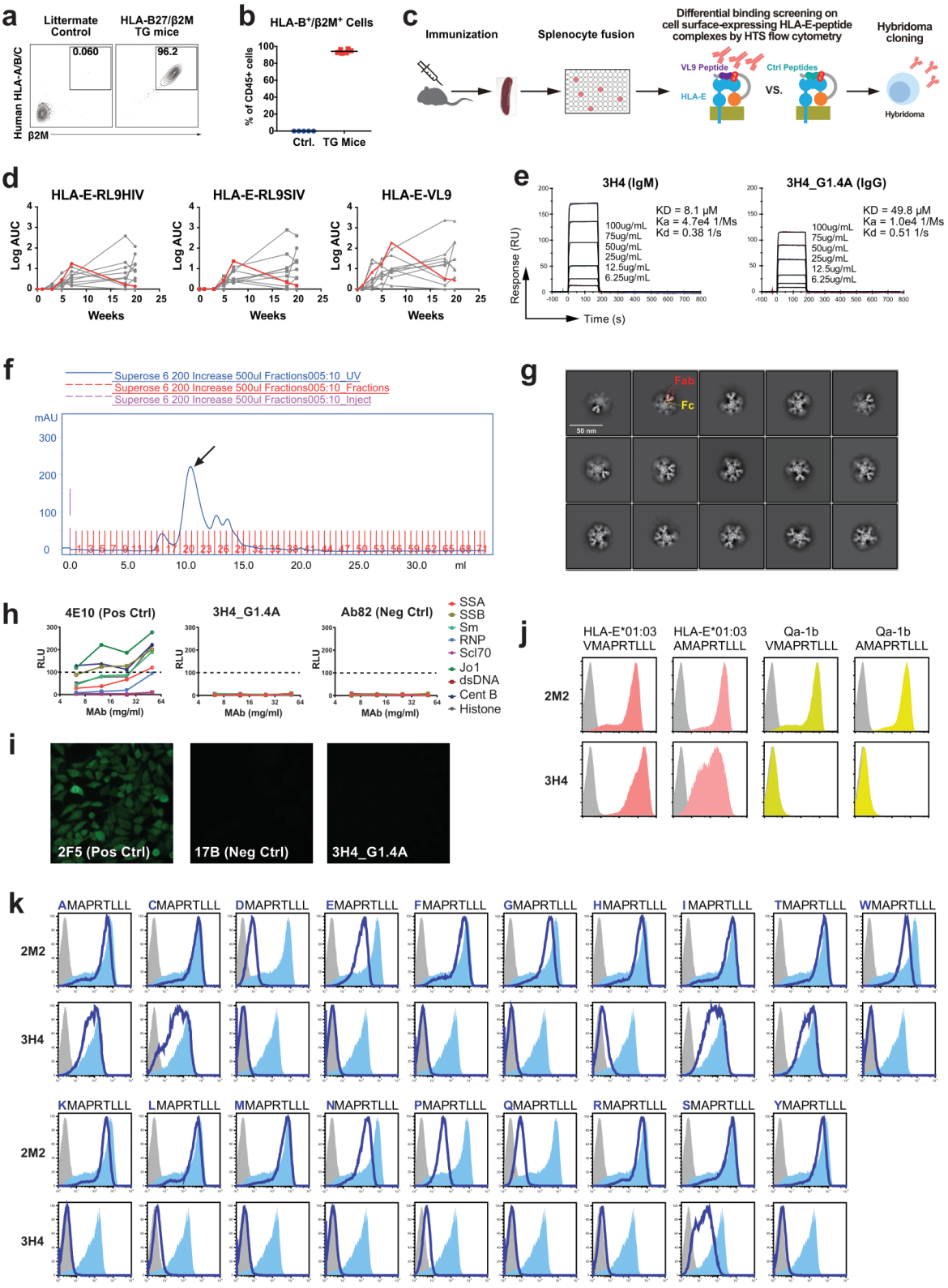

Figure. S1 Isolation and characterization of monoclonal antibody 3H4.

465 **a-b, Expression of human HLA-B27 and β2M in peripheral blood lymphocytes (PBLs)**
466 **of the transgenic (TG) mice.** HLA-B27/β2M TG mice were used to minimize the induction
467 of antibodies to HLA class I and β2M. Mouse PBLs from TG mice and littermate control were
468 isolated and stained with anti-mouse CD45, anti-human HLA class I (A/B/C) and anti-human
469 β2m antibodies. Representative data (a) and the percentages of human HLA-B27^{+}β2M^{+} cells
470 in CD45^{+} PBLs from TG mice (n=6) and control mice (n=6) (b) were shown.
471 **c, Schematic diagram of the immunization, splenocyte fusion and hybridoma**
472 **screening strategy.** HLA-B27/β2M TG mice (n=10) were immunized with cell surface-
473 expressing HLA-E-RL9 peptide (a peptide derived from HIV-1; denoted RL9HIV hereafter)
474 single-chain trimer (SCT)-transfected 293T cells (indicated by red arrows). After
475 immunizations, spleen cells were harvested from the selected mouse and the fusion was
476 performed using NS0 cells to generate hybridoma cells. Supernatants from the hybridoma
477 cell candidates were screened for differential binding by surface staining on HLA-E-VL9,
478 HLA-E-RL9HIV or HLA-E-RL9SIV transfected 293T cells. Hybridomas producing antibodies
479 specific for HLA-E-VL9 but not others were selected for cloning and downstream analysis.
480 Monoclonal cells were cloned for at least five rounds.
481 **d, Serum antibody binding ELISA.** Serum antibodies to HLA-E-VL9, HLA-E-RL9SIV, HLA-
482 E-RL9HIV complexes were quantified by ELISA and shown as log AUC (area under curve).
483 Antigens used for immunizations and ELISA assays are all cysteine (C)-trap stabilized. Each
484 curve represents one animal, and the curve for animal that we used for splenocyte fusion
485 are shown in red.
486 **e, Affinity of 3H4 binding to soluble HLA-E-VL9 complex.** 3H4 as a mouse IgM or as a
487 recombinant human IgG1 were immobilized on CM5 sensor chips and soluble HLA-E-VL9
488 complex protein at the indicated concentrations was flowed over antibody immobilized
489 sensor chips. Binding data are shown as black lines, and the best fits of a 1:1 binding model
490 are shown as colored lines. Rate constants (k_a, k_d) and dissociation constant K_D were
491 measured following curve fitting analysis.

492 **f, Purification of 3H4 by FPLC using Superose 6 size exclusion column.** The arrowed
493 peak was collected and analyzed by negative staining.
494 **g, Representative class average images of 3H4 negative stain electron microscopy**
495 **(NSEM).**
496 **h, Binding of 3H4 expressed in a human backbone G1.4A to a panel of autoantigens**
497 **by AtheNA assays.** HIV-1 gp41 antibody 4E10 was set as a positive control, and a Flu
498 antibody Ab82 was used as a negative control. The dotted lines indicate the cutoff values
499 ≥100 luminance units used to denote positivity.
500 **i, Binding of 3H4 in human backbone G1.4A to HEp-2 epithelial cells in indirect**
501 **immunofluorescence staining assays.** HIV-1 gp41 antibody 2F5 was set as a positive
502 control, and HIV-1 gp120 antibody 17B was used as a negative control. Antibody staining
503 concentration was 50 μg/ml, and data were collected at 40x objective for 8 seconds. Data
504 are representative from one of two independent experiments.
505 **j, 3H4 does not cross-react with mouse Qa-1b-peptide complex.** 293T cells were
506 transfected with HLA-E-VL9 (VMAPRTLLL), HLA-E-AL9 (AMAPRTLLL), mouse Qa-1b-VL9,
507 or mouse Qa-1b-AL9. Transfected cells were stained with 3H4 antibody or an anti-β2M
508 control antibody 2M2 followed by AF647 conjugated anti-mouse IgG(H+L) secondary
509 antibody. Data are representative from one of three independent experiments.
510 **k, 3H4 recognizes peptides with variants in P1**. 293T cells were transfected with HLA-E
511 SCTs with VL9 peptides with single amino acid mutations at P1, then stained with 3H4
512 antibody or an anti-β2M control antibody 2M2 followed by AF647 conjugated anti-mouse
513 IgG(H+L) secondary antibody (dark blue). Cells were gated for EGFP positive subsets.
514 Isotype control stained cells were used as a negative control (grey filled histograms), and the
515 wildtype VL9 peptide was a positive control (pale blue filled histograms). Data are
516 representative from one of three independent experiments.
517

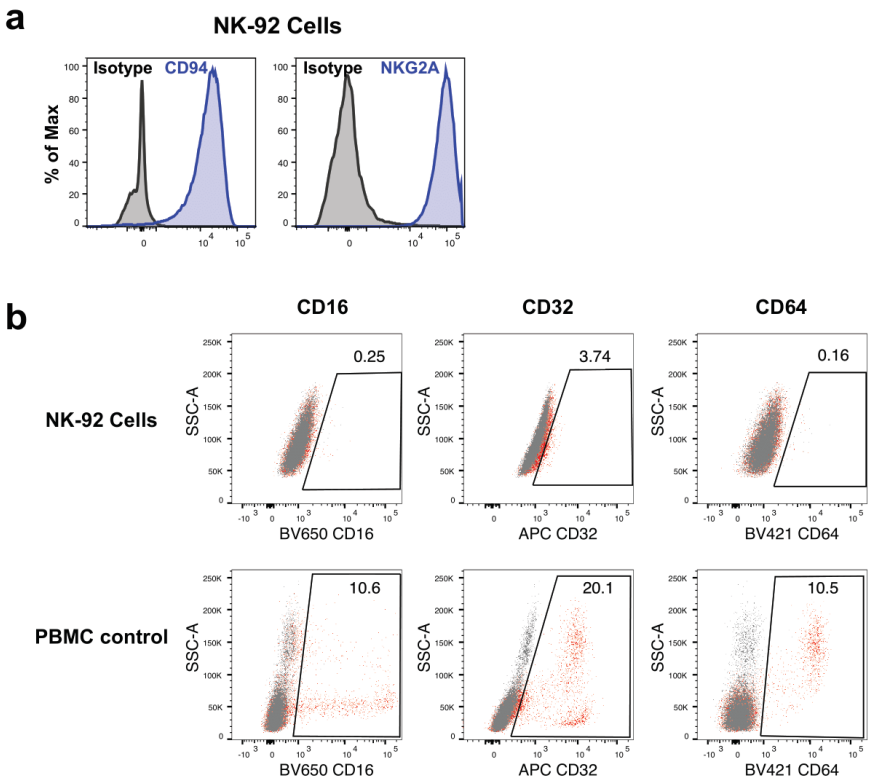

Figure. S2 Phenotypic analysis of NK-92 cells.

a, NKG2A and CD94 expression in NK-92 cell line detected by flow cytometry. NK-92 cells were stained with PE-CD94 antibody or FITC-NKG2A antibody and analyzed in flow cytometer. A PE-isotype and FITC-isotype antibodies were used as negative controls.

b, Fc receptors CD16, CD32 and CD64 expression in NK-92 cell line detected by flow cytometry. NK-92 cells were stained with BV650-CD16 antibody, APC-CD32 antibody, or BV421-CD64 antibody and analyzed in flow cytometer. Peripheral blood mononuclear cells (PBMCs) were used as positive controls. Dot plots overlay of antibody stained cells (red) and unstained control cells (grey) were shown. NK-92 cells were negative for CD16, CD32 or CD64, while a subset of PBMC cells were positive for each antibody. Data from a single antibody phenotype experiment.

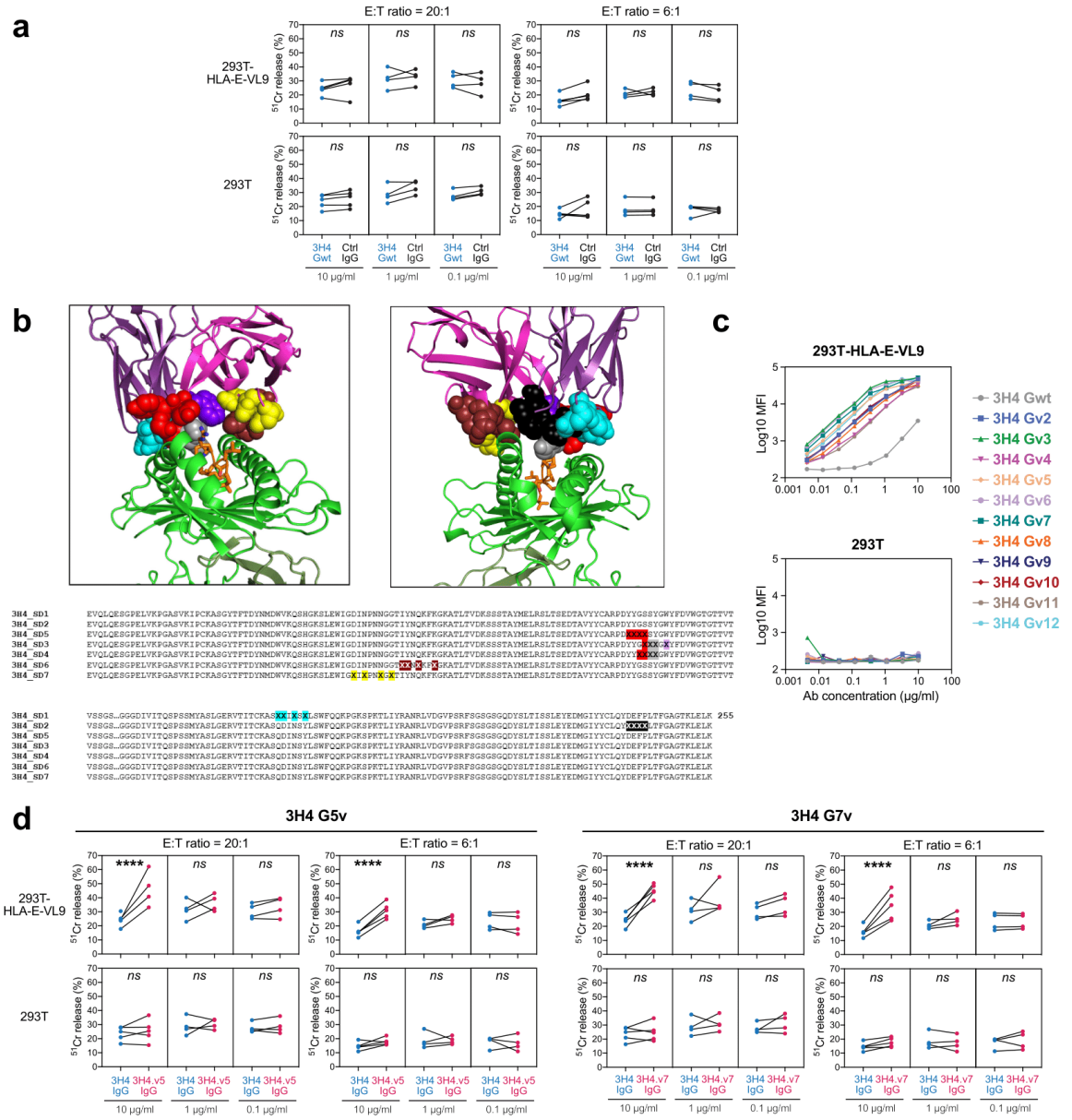

Figure. S3 Affinity optimization of 3H4 IgG.

a, NK cell cytotoxicity against wild-type 3H4 IgG-treated target cells measured by ^{51}Cr release assay. Unoptimized, wild-type 3H4 on a human IgG1 backbone (3H4 Gwt) was incubated with HLA-E-VL9 transfected 293T cells and untransfected 293T cells at final concentration of 10 μg/ml, 1 μg/ml, or 0.1 μg/ml, and NK92 cells were added into the mixture as effector cells at effector: target (E:T) ratios of 20:1 and 6:1. Human IgG1 CH65 was used as an isotype controls. Dots represent the mean values of triplicate wells in four or five independent experiments. Asterisks show the statistical significance between indicated groups: ns, not significant.

541 **b, 3H4 residues optimized for affinity improvements by library screening.** Seven
542 different libraries were designed that simultaneously sampled group of 4 amino acids in the
543 CDR loops of 3H4 that interact with HLA-E-VL-9 by structural analysis. *Top*: Structural
544 mapping of the amino acids (*spheres*) sampled together in the different libraries. Residues
545 shown in the same color were randomized together. HLA-E: *green*; VL-9: *orange*; *Bottom*:
546 Amino acid sequence of the seven 3H4 libraries, with randomized residues marked with '*X*'
547 and colored as in the structural panels above.
548 **c, Binding of wild-type 3H4 and variants on transfected 293T cells.** Wild-type 3H4 and
549 variants were titrated on HLA-E-VL9-transfected or untranfected 293T cells. Mean
550 fluorescent intensity (MFI) from one of three independent experiments were shown.
551 **d, Enhanced NK-92 cell cytotoxicity by optimized IgG 3H4 Gv5 and 3H4 Gv7 on HLA-**
552 **E-VL9 transfected 293T cells and untransfected 293T cells, in compare with IgG 3H4**
553 **Gwt.** Dots represent the mean values of triplicate wells in four or five independent ^{51}Cr
554 release assays. Statistical analysis was performed using mixed effects models. Asterisks
555 show the statistical significance between indicated groups: ns, not significant, *P<0.05,
556 **P<0.01, ***P<0.001, ****P<0.0001.
557

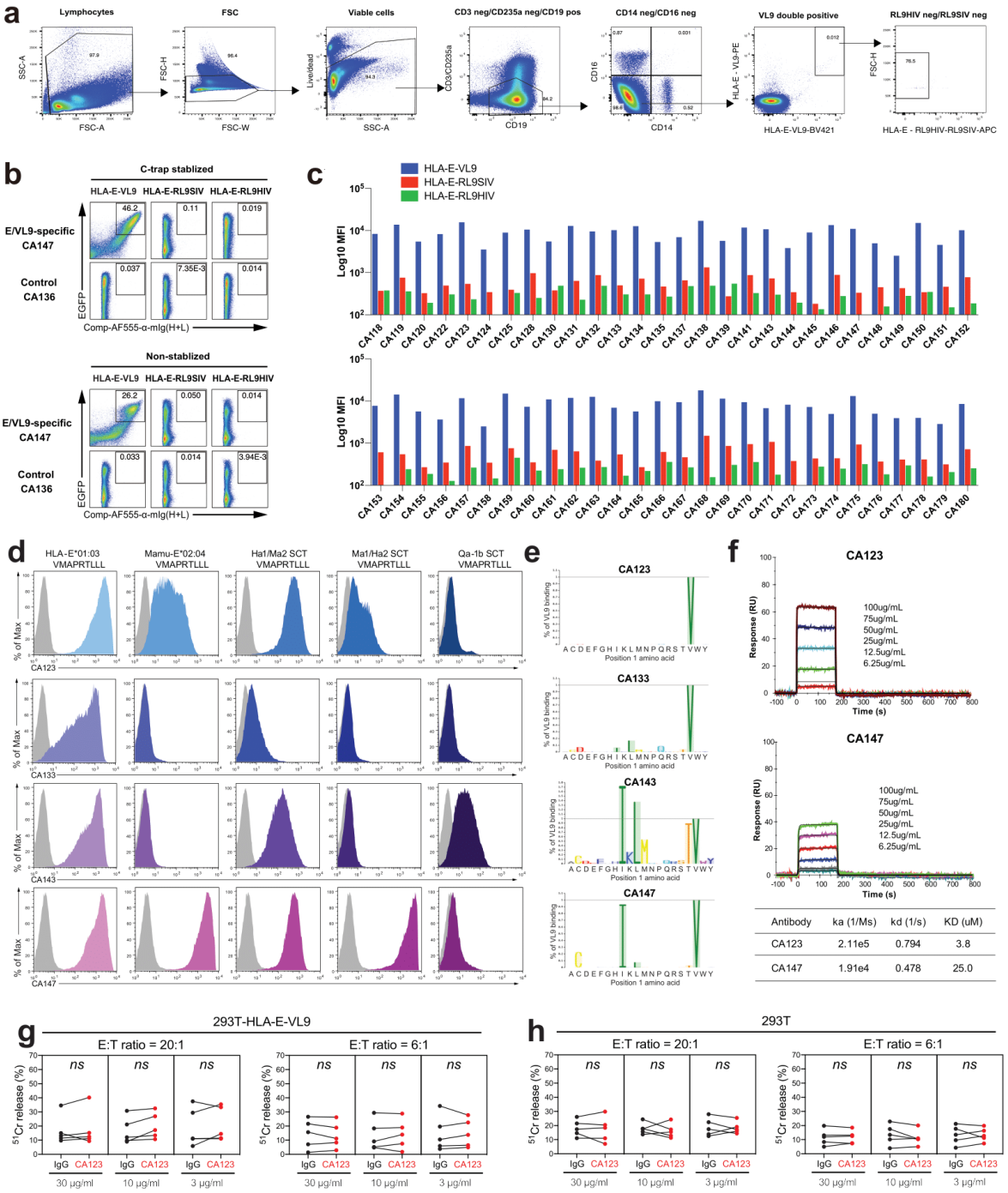

Figure. S4 Isolation and characterization of human HLA-E-VL9-specific antibodies.

a-b, HLA-E-VL9-specific B cell phenotyping from mice. Splenic cells isolated from HLA-B27/β2M TG mice (a) or C57BL/6 mice (b) were stained and analysed flow cytometry for B cells (B220+CD19+) that are HLA-E-VL9 double positive, HLA-E-RL9HIV negative and HLA-E-RL9SIV negative.

564 **c, Gating strategy of the single cell sorting for HLA-E-VL9-specific B cells from a**
565 **Cytomegalovirus (CMV)-negative, male human.** Human B cells were first enriched from
566 PBMCs by pan-B cell negative selection magnetic beads. The enriched cells were stained
567 and gated on viable/CD14^{neg}/CD16^{neg}/CD3^{neg}/CD235a^{neg}/CD19^{pos}/HLA-E-VL9^{pos}/HLA-E-
568 RL9HIV^{neg}/ HLA-E-RL9SIV^{neg} subset as shown. Cells were single-cell sorted into 96-well
569 plates for the downstream PCR cloning. Representative data from one of the four donors
570 were shown.
571 **d-e, Flow cytometry titration of purified HLA-E-VL9-specific mAbs isolated from a**
572 **CMV-negative, male human.** Antibodies recovered from sorted B cells were constructed in
573 human IgG1 backbones and used for staining titration on both C-trap-stabilized and
574 unstabilized HLA-E-VL9, HLA-E-RL9SIV, HLA-E-RL9HIV transfected 293T cells. EGFP
575 expression indicates transfection efficiency. Transfected cells were stained with testing
576 antibodies at the concentration of 2 μg/ml, followed by secondary antibody AF555-anti-
577 human IgG staining. (d) Staining data of a representative antibody CA147 and a negative
578 control antibody CA136. (e) Summary of the MFI of antibody binding data shown as bar
579 chart. Data are representative from one of two independent experiments.
580 **f, Cross-reactivities of human HLA-E-VL9 antibodies with rhesus Mamu-E-VL9 and**
581 **mouse Qa-1b-VL9 complex.** 293T cells were transfected with HLA-E-VL9, Mamu-E-VL9,
582 two HLA-E/Mamu-E hybrids [HLA-E α1/Mamu-E α2 (Hα1/Mα2) and Mamu-E α1/HLA-E α2
583 (Mα1/Hα2)], and Qa-1b-VL9. Transfected cells were stained with human antibodies CA123,
584 CA133, CA143, and CA147, followed by AF647 conjugated anti-mouse IgG(H+L) secondary
585 antibody. Data are representative from one of three independent experiments.
586 **g, Mapping of representative HLA-E-VL9-specific mAbs CA123, CA133, CA143 and**
587 **CA147 on 293T cells transfected with HLA-E-VL9 peptide variants.** 293T cells were
588 transfected with HLA-E SCTs with VL9 peptides with single amino acid mutations at P1, then
589 stained with human antibodies CA123, CA133, CA143, and CA147, followed by AF647
590 conjugated anti-mouse IgG(H+L) secondary antibody (dark blue). Cells were gated for EGFP
591 positive subsets. MFI of the indicated antibody staining on wildtype VL9 peptide was set as

592 100%, and the percentages equals to (MFI of binding on each P1 variant) / (MFI of binding
593 on wildtype VL9) x 100%.
594 **h, Affinity measurements of human HLA-E-VL9 antibodies binding to soluble HLA-E-**
595 **VL9 complex.** Human antibodies CA123 or CA147 on human IgG1 backbone was
596 immobilized on CM5 sensor chips and soluble HLA-E-VL9 complex protein at the indicated
597 concentrations was flowed over the antibody immobilized sensor chips. Rate constants (k_a,
598 k_d) and dissociation constant K_D were measured following curve fitting analysis.
599 **i-j, NK cell cytotoxicity against CA123 IgG-treated target cells as assessed by ^{51}Cr**
600 **release assay.** Human antibody CA123 was incubated with HLA-E-VL9 transfected 293T
601 cells (i) and untransfected 293T cells (j) at final concentration of 30 μg/ml, 10 μg/ml or 3
602 μg/ml, and NK92 cells were added into the mixture as effector cells at effector: target (E:T)
603 ratio of 20:1 and 6:1. Human antibody A32 were used as the isotype control. Dots represent
604 the mean values of triplicate wells in five independent experiments. Statistical analysis was
605 performed using mixed effects models.
606

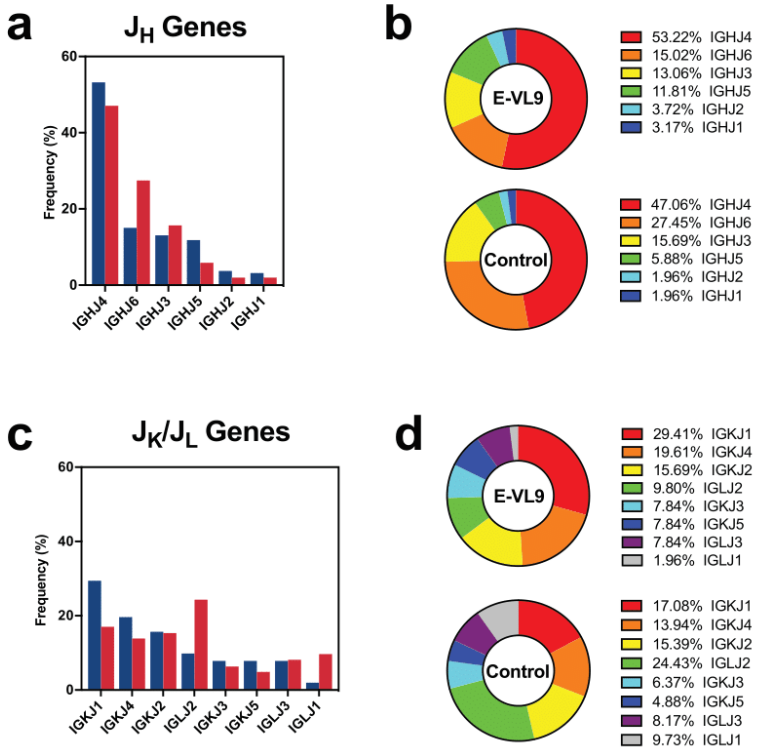

Figure. S5 J chain sequence analysis of HLA-E-VL9-specific antibodies (n=51). Reference VH-VL repertoires (n=198,148) from three healthy humans from a previous study (DeKosky et al., 2015) was used as a control.

a-b, Heavy chain (J_H) gene usage shown as bar chart (a) and pie chart (b).

c-d, Kappa chain (J_k) and lambda chain (J_L) gene usage shown as bar chart (c) and pie chart (d).

615 **SUPPLEMENTAL TABLES**

616

617 **Table S1. Gene usage and mutation rate of four HLA-E-VL9-specific mAbs isolated**

618 **from immunized transgenic mice.**

619

620 **Table S2. Crystallographic data for the 3H4 Fab and VL9-bound HLA-E co-complex**

621 **structure.**

622 **a, Crystallographic data collection and refinement statistics.** AS: Ammonium sulphate.

623 § r.m.s.d.: root mean square deviation from ideal geometry. Statistics for outer shell

624 indicated in parentheses. AU: asymmetric unit. Rfree equals the R-factor against 5% of the

625 data removed prior to refinement.

626 **b-f, Inter-chain RMSD and inter-molecular interfaces in the 3H4-HLA-E-VL9 structure.**

627 **b,** Table detailing the total buried surface area of the interface in $Å^2$ between the 3H4 VH, VL

628 and the VL9-bound HLA-E complex. **c,** Table of RMSD (root mean square deviation) in Å

629 between chains of the 3H4-HLA-E-VL9 co-complex structure. Two copies of the 3H4 Fab-

630 HLA-E-VL9 co-complex were present in the asymmetric unit and thus RMSD between

631 chains related by non-crystallographic symmetry was calculated via Cα atom pairwise

632 alignment on the PDBePISA server. Average Cα atom RMSD following pairwise alignment is

633 also reported for the HLA-E heavy chain (HC) of 1MHE (Chain A), a previously published

634 non-receptor-bound VL9-loaded HLA-E complex, and the HLA-E HC from the 3H4-HLA-E-

635 VL9 structure reported here (Chain A). **d,** Table listing residues involved in the interface

636 between the 3H4 VH and the VL9 peptide. **e,** Table of interacting residues of the 3H4 VH

637 and HLA-E HC interface. **f,** Table of interacting residues of the 3H4 VL and HLA-E HC

638 interface.

639 **g-h, Hydrogen bonding and salt bridges in the 3H4-HLA-E-VL9 structure.** Table of

640 hydrogen bonds and salt bridges formed between the 3H4 heavy chain (HC) and the HLA-E

641 HC (**g**) and the 3H4 light chain and the HLA-E HC (**h**).

642 *Hydrogen bonding cut-offs according to the PDBePISA default criteria. 3H4 chain numbering*

643 *is according to the Kabat scheme whereby alternate insertion codes (letters after the residue*
644 *number) are added to variable length regions of the antibody sequence. 3H4 residues within*
645 *the CDRs are shaded green and labelled 'CDR1/2/3'. The position of HLA-E HC residues*
646 *either on the α1 or α2 helix is also noted. Amino acid atom abbreviations: C - mainchain*
647 *Carbon atom, O - mainchain Oxygen atom, N - mainchain Nitrogen atom, CA - α-Carbon*
648 *atom, CB - β-Carbon atom, CD - δ-Carbon atom, CE - ε-Carbon atom, CG - γ-Carbon atom,*
649 *CH - η-Carbon atom,, CZ - ζ-Carbon atom, OD - δ-Oxygen atom, OE - ε-Oxygen atom, OG -*
650 *γ-Oxygen atom, OH - η-Oxygen atom, ND - δ-Nitrogen atom, NE - ε-Nitrogen atom, NH - η-*
651 *Nitrogen atom, NZ - ζ-Nitrogen atom.*
652
653 **Table S3. Information of human subjects used in this study.**
654
655 **Table S4. HLA-E-VL9-specific antibodies isolated from human.** Index sorting MFI,
656 immunogenetics information, and transfected 293T cell staining MFI of the 60 HLA-E-VL9-
657 specific antibodies isolated from single B cell sorting were shown. The original isotypes of all
658 the antibodies were IgMs. Antibodies from the same clonal family were highlighted in yellow.
659